REPORT

Fate of nitrate during groundwater recharge in a fractured karst aquifer in Southwest Germany

Anna-Neva Visser [1,2] · Moritz F. Lehmann [1] · Hermann Rügner [2] · Fernando Mazo D'Affonseca [2] · Peter Grathwohl [2] · Nia Blackwell [2] · Andreas Kappler [2] · Karsten Osenbrück [2]

Abstract

Over the past decades, fractured and karst groundwater systems have been studied intensively due to their high vulnerability to nitrate (NO_3^-) contamination, yet nitrogen (N) turnover processes within the recharge area are still poorly understood. This study investigated the role of the karstified recharge area in NO_3^- transfer and turnover by combining isotopic analysis of NO_3^- and nitrite (NO_2^-) with time series data of hydraulic heads and specific electrical conductivity from groundwater monitoring wells and a karstic spring in Germany. A large spatial variability of groundwater NO_3^- concentrations (0.1–0.8 mM) was observed, which cannot be explained solely by agricultural land use. Natural-abundance N and O isotope measurements of NO_3^- ($\delta^{15}N$ and $\delta^{18}O$) confirm that NO_3^- derives mainly from manure or fertilizer applications. Fractional N elimination by denitrification is indicated by relatively high $\delta^{15}N$- and $\delta^{18}O$-NO_3^- values, elevated NO_2^- concentrations (0.05–0.14 mM), and $\delta^{15}N$-NO_2^- values that were systematically lower than the corresponding values of $\delta^{15}N$-NO_3^-. Hydraulic and chemical response patterns of groundwater wells suggest that rain events result in the displacement of water from transient storage compartments such as the epikarst or the fissure network of the phreatic zone. Although O_2 levels of the investigated groundwaters were close to saturation, local denitrification might be promoted in microoxic or anoxic niches formed in the ferrous iron-bearing carbonate rock formations. The results revealed that (temporarily) saturated fissure networks in the phreatic zone and the epikarst may play an important role in N turnover during the recharge of fractured aquifers.

Keywords Nitrate · Karst · Groundwater recharge · Stable isotopes · Germany

Introduction

Contamination of karstified aquifers is of major concern since these systems supply up to 25% of the world's population with drinking water (Ford and Williams 2007). Karst aquifers are known to be particularly vulnerable to anthropogenic contaminants such as nitrate (NO_3^-) (Einsiedl and Mayer 2006; Katz 2012; Husic et al. 2019). Karstified groundwater systems mainly develop via the natural dissolution of carbonate rocks (i.e., limestones, dolomites) resulting in the formation of a heterogeneous flow system characterized by sink holes,

sinking streams, caves, fractures and fissures. Water flow within the system is modulated by highly permeable karst structures (enlarged fractures and conduits), as well as the less permeable rock matrix (small pores and fissures) (Ford and Williams 2007; Hartmann et al. 2014). The conduit network allows rapid response to rain events, resulting in quick intrusion of surface water (and potentially also pollutants) into the aquifer, as well as rapid transport within it (Einsiedl 2005; Pronk et al. 2006). Although the sources of nitrogen (N) inputs for non-karstified and karstified aquifers are similar (e.g., agriculture, waste water; Wakida and Lerner 2005; Matiatos 2016), N pathways in karst systems were shown to be much more diverse due to heterogeneous flow pathways (Husic et al. 2019).

While fissure and fracture networks, particularly the epikarst zone, have been shown to play a major role in storing and locally rerouting vertical infiltrating waters (Jones 2003), they are also known to promote the formation of zones of enhanced biological activities (Pipan and Culver 2007; Lian

✉ Karsten Osenbrück
karsten.osenbrueck@uni-tuebingen.de

[1] Basel University, Biogeochemistry, Bernoullistrasse 30, 4056 Basel, Switzerland

[2] Centre for Applied Geoscience, Tübingen University, Schnarrenbergstrasse 94-96, 72076 Tübingen, Germany

et al. 2011). Hence, besides processes occurring within the overlying soil (e.g., Munch and Velthof Gerard 2007), N turnover is also mediated by terrestrially derived and sediment-bound microbial communities present within the karstified system (Simon and Benfield 2002; Heffernan et al. 2012; Henson et al. 2017). Previous studies showed that bacterial communities located either in caves or the major conduit network can drive various reactions such as mineralization, immobilization, nitrification and denitrification (Farnleitner et al. 2005; Katz 2012; Henson et al. 2017). For example, Herrmann et al. (2017) provided evidence for the presence of denitrifying bacterial communities suspended in groundwater monitoring wells and/or attached to the parent rock matrix of a limestone aquifer. Which process is favoured by the microbial community (and in turn the fate of e.g., fixed N) strongly depends on the availability of suitable electron donors (e.g., organic carbon or ferrous iron bearing minerals such as pyrite), as well as the ambient redox conditions (Henson et al. 2017; Herrmann et al. 2017).

Natural abundance measurements of NO_3^- and NO_2^- isotope ratios (^{15}N and ^{18}O) represent a powerful tool to gain deeper insights into the sources and fate of fixed (i.e., bioavailable) N in groundwater. Common pollutant sources of NO_3^- in groundwater (e.g., soil-N, manure, synthetic fertilizer and sewage effluents) have distinct isotopic signatures, which can be used to semiquantify the relative importance of the single N sources (Panno et al. 2001; Katz et al. 2004; Musgrove et al. 2016; Vystavna et al. 2017). At the same time, N compounds do not necessarily behave conservatively in groundwater, and processes such as denitrification have been demonstrated to alter the primary isotopic signatures in, e.g., karstic systems (Panno et al. 2001; Einsiedl et al. 2005; Husic et al. 2020). In turn, the N and O isotopic signatures of NO_3^- (and other dissolved N species) can be used to assess various N turnover processes in groundwater (Kendall and Aravena 2000; Einsiedl and Mayer 2006; Grimmeisen et al. 2017). So far, most groundwater studies focused on the investigation of N and O isotopic signatures of NO_3^-, since concentrations of intermediates such as NO_2^- are commonly low (e.g., Herrmann et al. 2017). The few field studies that also included isotope analyses of NO_2^- (Smith et al. 2004; Wells et al. 2016) demonstrated that multi-species measurements provided additional process-level insight in N transformation pathways. The dual N and O isotope approach for both, NO_3^- and NO_2^-, is based on the fact that during most biotic N-elimination processes, the lighter N and O isotopologues are preferred, resulting in distinct parallel enrichment of the heavy isotopes (i.e., ^{15}N, ^{18}O) of the remaining pool of NO_x-species (Kendall and Aravena 2000; Granger et al. 2008). In contrast, NO_3^- regeneration may lead to a differential behaviour of the NO_3^- and NO_2^- isotope ratios, and thus allows to disentangle NO_3^--producing and consuming processes when they occur simultaneously (e.g., Lehmann et al. 2004; Granger and Wankel 2016), in, for example, the recharge zones of karst aquifers.

How N turnover in the recharge areas of karst aquifers contributes to NO_3^- elimination along the flow path, remains unclear (Jones and Smart 2005; Musgrove et al. 2016; Husic et al. 2019). Therefore, the main goal of this study was to investigate possible causes promoting NO_3^- variability within the recharge area of karst groundwater systems, and thus to unravel the particular role of the recharge area and epikarst zone with regard to NO_3^- transfer, turnover, and storage. To achieve this goal, natural-abundance isotope ratio measurements of NO_3^-, as well as of NO_2^- ($\delta^{15}N$ and $\delta^{18}O$), were combined with hydraulic, hydrochemical and biogeochemical approaches. Many studies investigating N turnover processes in karstified aquifers focussed on the larger conduit network (i.e., spring-based studies), and thus on compartments that are known to quickly respond to rain events (e.g., Birk et al. 2004; Kaufmann et al. 2014; Asante et al. 2018). In order to capture the occurring N transport processes, the presented study focuses on several groundwater monitoring wells, which are connected to different flow paths within a fractured and karstified aquifer, but are not dominated by karst conduits; for comparison, one of the main springs of the karst aquifer was also examined. The sampling locations were situated in the recharge area of a karstified and fractured limestone aquifer in SW Germany, which is characterised by a high variability in NO_3^- concentrations.

Materials and methods

Study catchment

The studied fractured and karstified Upper Muschelkalk aquifer is situated in the "Oberes Gäu", a landscape within the Southwest German Triassic Scarp lands, located approximately 30 km southwest of Stuttgart. Part of this regional aquifer underlies the catchment of the River Ammer, which originates from karstic springs close to the town of Herrenberg. The focus of this study is on the ~30 km² large western section of the aquifer, situated west of Herrenberg (Fig. 1a). Due to outcropping of the carbonate rocks of the Upper Muschelkalk, this region constitutes the main recharge area to the groundwater system (Fig. 1b). Topographically, the area forms a slightly undulating plateau with small but steeply incised valleys dipping towards the Ammer Valley in the southwest (Fig. 1c). The elevation ranges from 400 to 590 m asl between the Ammer springs and the plateau. The overlying soils are usually shallow (0.3–1.8 m) and consist partly of loess, rendzinas developed from carbonate rocks, and more clayey soils in places where mudstones of the Lower Keuper formation cover the Muschelkalk. Karstification of the Upper Muschelkalk

Fig. 1 **a** Location of the study area close to the town of Herrenberg in Germany (DE) [country codes from https://www.iso.org/obp/ui]; **b** lithostratigraphic map of the study area with the four major field sites (Sulz am Eck (Sul), Haslach (Has), Ammer springs (AMQs), and the artesian well Altingen (ArtAlt)), based on the Gauß-Krüger coordinate system; the dotted black line indicates the cross section below; **c** geological cross section of the main geological formations in the study area, including the major field sites
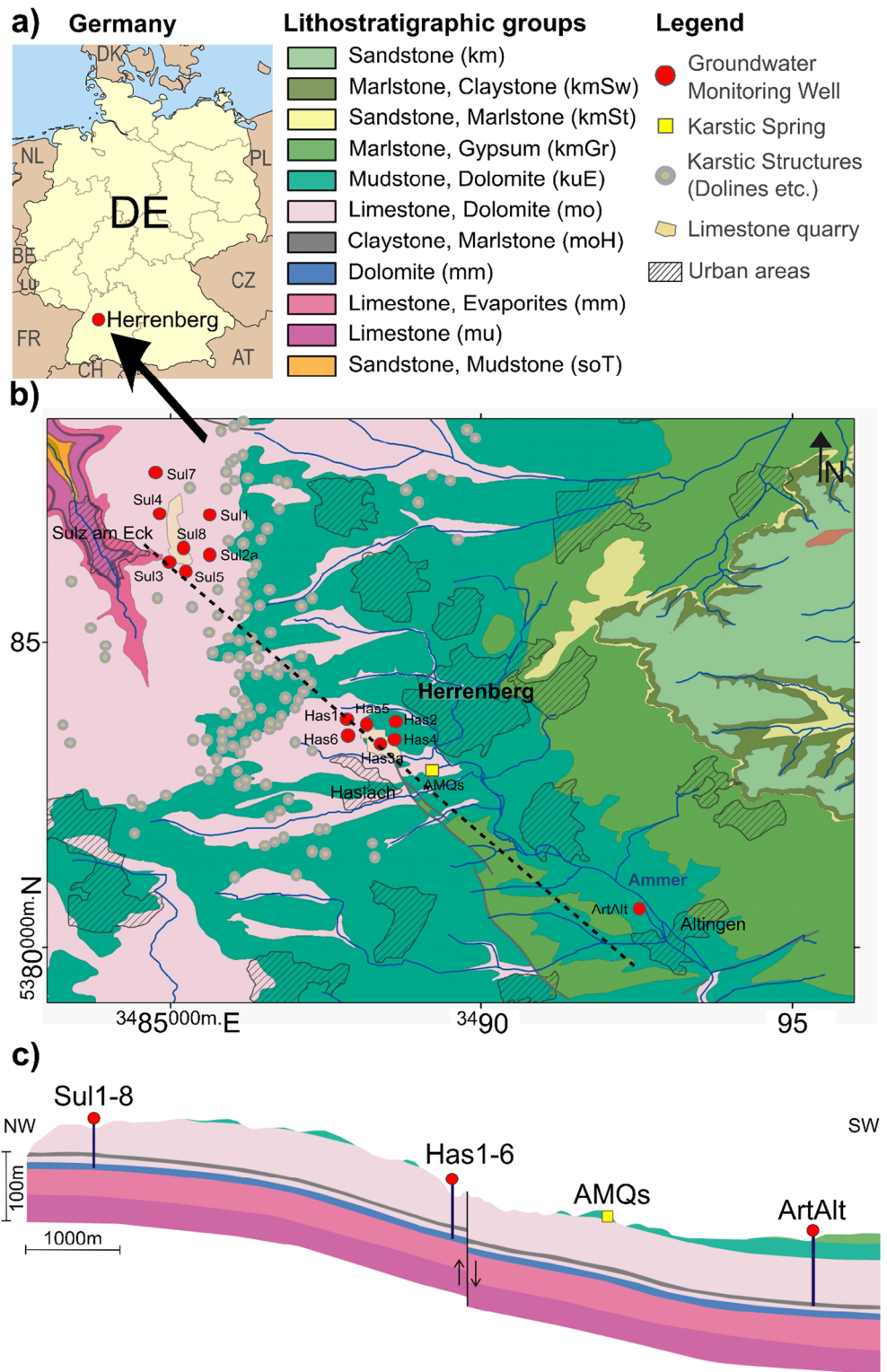
formed numerous dolines within the study area (see Fig. 1b), providing pathways for rapid infiltration of water to greater depths. Other karstic structures present in the study area include dry valleys, stream sinkholes, and two major karstic springs (i.e., Ammer springs 1 and 2 (AMQs); see Fig. 1b,c).

Mean annual precipitation for the studied period 2015 to 2018 at stations nearby (Herrenberg and Bondorf) range between 550 and 690 mm/year, and the average annual temperature was 9.9 °C, which is about 1.9 °C higher than the long-term mean value since the 1980s. Estimates of mean annual

groundwater recharge rates (20-year average) range between 200 and 300 mm/year (LUBW 2016; D'Affonseca et al. 2020).

Access to the groundwater is provided via the karstic springs (Ammer springs, AMQs), six groundwater monitoring wells near Haslach (Has1-Has6), and seven groundwater monitoring wells near Sulz am Eck (Sul1-Sul8), which were used for physical and chemical monitoring. An additional artesian monitoring well (ArtAlt) in the confined part of the aquifer east of the town of Herrenberg was investigated for comparison. The AMQs consist of at least two large pools (elevation 403 m asl), where groundwater is directly upwelling from the uncovered Muschelkalk rocks with an average discharge of about 40–50 L/s. Due to the location of the monitoring wells in Haslach and Sulz on the plateau (elevation 436–588 m asl), groundwater levels at these wells ranged between 35 and 100 m below the surface (490–515 m asl). All wells have diameters of 10.2 or 12.7 cm, and screened sections ranging from 8 to 10 m length, except for the deepest wells in Sulz featuring a longer screen length of 20 m.

Land use at the study site is dominated by agriculture (about 67%), followed by urbanized areas (about 15%), and forested land (about 18%) (Grathwohl et al. 2013; Liu et al. 2018). Intense agriculture leads to the release of NO_3^- and other compounds into the karstic groundwater system. Other possible sources of N-contaminants include leakages from sewer systems from farms or urban areas; however, the majority of which are located downgradient of the monitoring wells. Two operating quarries of 0.16 and 0.24 km^2 at the plateau (location see Fig. 1b) provide access to the carbonate rocks of the Muschelkalk aquifer, allowing rock samples to be taken from freshly exposed rock faces. The study area is part of a large water protection zone, supplying more than 150,000 people with drinking water from the Upper Muschelkalk aquifer.

Geological and hydrogeological setting

The study area (see Fig. 1b) is dominated by Triassic rock formations of the Upper Muschelkalk and the Lower and Middle Keuper. Quaternary deposits (alluvial-fan and floodplain sediments from the Holocene) are only present in the valley of the Ammer River. The Upper Muschelkalk is composed of fractured and partly karstified limestones and dolomites with a total thickness of 80–90 m (Villinger 1982). The base of the aquifer is formed by porous to cavernous dolomites and dolomitic marls, overlying clayey subrosion residues of the evaporite-dominated formations of the Middle Muschelkalk. In large parts, the Upper Muschelkalk consists of a series of micritic limestones of low porosity (0.5–5.0%). A typical feature of the Muschelkalk formation is ferrous iron bearing limestones and dolostones. Within the limestone matrix, small pyrite

crystals (FeS_2) can be frequently found with concentrations of up to 2 mass-%. The organic carbon content of the limestones is generally low with <0.06 mass-%. The upper 15–20 m of the Upper Muschelkalk consist of porous (15–30%) or partly cavernous dolomites and dolomitic limestones interbedded with thin marl layers of constant thickness (Trigonodus Dolomite).

The fractured and fissured limestone and dolomite rocks of the Upper Muschelkalk can be characterized as partly karstified. Former fluorescent tracer tests showed that the karstic springs are connected to major karst conduits (Harreß 1973). In addition to karstic features, regional groundwater flow is influenced by numerous tectonic structures comprising conjugated fault patterns formed by two large synthetic WSW–ENE fault zones, with antithetic SE–NW faults in between (D'Affonseca et al. 2020).

The Upper Muschelkalk outcrops in the study area and gently dips to the SE, where it is increasingly covered by claystones, dolomites, sandstones, and marlstones of the Lower Keuper (Fig. 1b,c), which leads to unconfined conditions on the plateau whereas towards the SE the Muschelkalk aquifer becomes confined or even artesian (D'Affonseca et al. 2020). Generally, the groundwater flow direction is from NW to SE following the dipping of the Triassic formations. In the lower part of the Upper Muschelkalk, a 6–8 m thick, marlstone-claystone sequence (Haßmersheimer layers) hydraulically separates the aquifer into a basal and an upper part (Villinger 1982; Ufrecht and Hölzl 2006).

Groundwater monitoring and sampling

In December 2015, six automatic probes and data-loggers (CTD Diver, Schlumberger) were installed in selected monitoring wells (Has2, Has4, Has5, Sul1, Sul3, Sul4) to continuously record pressure (hydraulic head, H; range: 0–10 m; error: ±0.1%; resolution: 0.2 cm), water temperature (Tw; range: -20 to +60 °C; error: ±0.1 °C; resolution: 0.01 °C), and specific electrical conductivity (SEC; range: 0–120 mS/cm; error: ±1%; resolution: 1 μS/cm) at intervals of 30 min. Additionally, oxygen probes (miniDO$_2$T, PME) were installed in the same monitoring wells to measure dissolved oxygen (DO; range: 0–150% saturation; error: ± 5%; resolution: 0.1 mg/L) in groundwater at intervals of 30 min. The oxygen probes were deployed from Dec 2015 to Jun 2016 for Has4, Sul3, and Sul4, and from Dec 2015 to Mar 2017 for Has5 and Sul1, respectively. Unfortunately, the DO probe in well Has4 had to be installed close to the bottom of the well to ensure permanent water coverage, and due to sporadic sediment contact of the probe near the bottom DO data were compromised. Larger than expected water-table fluctuations in the range of 30 m led to pressure maxima in Feb/Mar 2016 and particularly in Jan 2018, which exceeded the maximum permissible value of the probe. Therefore, the CTD probes in

all wells were replaced in Feb 2018 by new probes (4 TD and 2 CTD Diver, Schlumberger), with an extended measurement range of up to 50 m water column.

Groundwater samples for chemical analysis (major ions, dissolved N compounds) were taken at the monitoring wells in the groundwater recharge area in three different sampling campaigns in Aug 2014, Apr 2016, and Jan 2018. The Apr 2016 campaign also included sampling for isotopic analysis ($\delta^{15}N$, $\delta^{18}O$ of NO_3^- and NO_2^-). Additional data on major ions including NO_3^- were available from a previous sampling campaign in Sep 2010. Data on groundwater chemistry from the karstic Ammer spring (AMQ) and the artesian well (ArtAlt) downgradient of the recharge area were used for comparison.

Different submersible pumps were used for sampling the monitoring wells depending on the diameter of the wells (10.2 or 12.7 cm) and the available water column. The pumps were usually operated with pumping rates between 0.01 and 0.20 L/s. Groundwater samples were taken after exchanging the water volume inside the well at least 1.5 times. Dissolved oxygen, pH, Tw and SEC were measured in the field using handheld probes (WTW GmbH, DO resolution 0.1%, accuracy ± 0.5% of value; pH accuracy ± 0.1% of value; SEC range 0.0 to 500 µS/cm, error: ± 0.5% of value; Tw range −5.0 to +105.0 °C, error: ±0.1 K) inserted to a flow-through cell, which was directly connected to the pump via PVC or PTFE tubes of 50–100 m length. Due to the relatively low pumping rates in some wells, the measured water temperatures were up to 5 °C higher compared to the original water temperature and were therefore not used for interpretation.

Water samples from the Ammer spring were collected as grab samples directly at the outlet. Groundwater samples from the artesian well ArtAlt were either taken from the artesian outflow or by using a submersible pump when the pressure head dropped below the well top during the summer season.

Capture zone delineation

Capture zones of the groundwater monitoring wells were determined by means of backward particle tracking using a recently established numerical groundwater flow model for the Muschelkalk aquifer (D'Affonseca et al. 2020). The code MODFLOW NWT (Niswonger et al. 2011), an autonomous version of the three-dimensional (3D) code of finite differences MODFLOW-2005 (Harbaugh 2005), was employed to simulate the regional flow regime within the aquifer, assuming steady-state conditions for simplicity. Using the groundwater flow data simulated by this model, conservative advective mass transfer calculations were conducted to estimate the capture zones of the monitoring wells by backward particle tracking with MODPATH, a MODFLOW post-processing module developed to calculate 3D flow paths (Pollock David 1994). In order to avoid setting particles into

dry cells, particles started near the filter screen bottom of each considered monitoring well. The starting point consisted of a horizontal circle of 0.3 m in radius containing 1,000 particles.

Solute concentration measurements

NO_3^- and NO_2^- concentrations were determined by standard spectrophotometric methods using a continuous flow analyser (CFA, Seal Analytics AA3), equipped with an additional set of pre-mounted membranes to filter out precipitates. Briefly, NO_2^- is reacted with an acidic sulphanilamide (SAN) solution forming a diazonium ion which binds to the N-1-napthylethylenediamine dihydrochloride solution (NEDD), resulting in a pinkish colorimetric complex (azo dye), detectable at 540 nm. NO_3^- is reduced first by a hydrazine sulphate solution and total NO_x ($NO_3^- + NO_2^-$) is determined. NO_3^- is quantified by subtracting the NO_2^- from NO_x (Sawicki and Scaringelli 1971); additionally, most ions were quantified by ion chromatography (Thermo Scientific Dionex DX-120, ANIONS: Dionex IonPac A523 analytical column with a Dionex IonPac AG23 guard column; CATIONS: Dionex IonPac CS12A-5 µm analytical column with a Dionex IonPac CG12A-5 µm guard column; LOQ = 0.1 mg/L). In order to determine the concentrations of the single iron species, a modified ferrozine assay, using 40 mM amidosulfonic acid (SFA) instead of 1 M HCl (Stookey 1970; Klueglein and Kappler 2013) was applied. The samples were diluted 1:10 in 1 M HCl at the field site, and then directly pipetted into a 96 well plate or in 1 ml cuvettes, respectively. Following the ferrozine assays protocol, the samples were photometrically at 562 nm (Thermo Scientific Multiskan GO).

Nitrate and nitrite isotope analysis

Natural abundance measurements of N and O isotope ratios in NO_3^- were performed using the denitrifier method (Coplen et al. 2004; Granger et al. 2006; Granger and Sigman 2009). Briefly, NO_3^- is enzymatically converted to N_2O by *P. aureofaciens*, which is then purified and analysed using a modified purge-and-trap gas bench coupled to a CF-IRMS (Thermo Scientific IRMS Delta V; McIlvin and Casciotti 2010). Blank contribution was generally lower than 0.3 nmol (as compared to 7 nmol of sample). Oxygen isotope exchange with H_2O during the reduction of NO_3^- to N_2O was corrected for, and was never higher than 5%. Isotope values were calibrated by standard bracketing using internal and international NO_3^- isotope standards with known N and O isotopic composition, namely IAEA-NO-3, USGS32, USGS34. For NO_2^- $\delta^{15}N$ and $\delta^{18}O$ isotope analysis a modified azide method was applied (McIlvin and Altabet 2005). This method is based on the chemical conversion of NO_2^- to N_2O using a 1:1 mixture of 2 M NaN_2 and 45% acetic acid (99.999%, Sigma Aldrich). In order to decrease oxygen exchange during chemical reaction, 0.6 M NaCl was added to

the acetic azide mix (McIlvin and Altabet 2005). Samples (targeting 7 nmoles of NO_2^-) were added to 12 ml vials, which were then closed with grey butyl stoppers and crimp sealed. Under a fume hood, the acetic acid/azide mix (100 µl per 3 ml sample) was added to each vial with a syringe. The next morning, 100 µl of a 10 M NaOH was added to stop the reaction. Until measurement (CF-IRMS, see the preceding), the samples were stored in the dark and upside down. For calibration, NO_2^- isotope standards —N-7373 and N-10219 (Casciotti and McIlvin 2007)—were prepared on the day of isotope analysis and processed the same way as samples. All N and O isotope data are expressed using the common δ notation and given in permille deviation (‰) relative to AIR N_2 and VSMOW, respectively $[(\delta^{15}N = ([^{15}N]/[^{14}N])_{sample}/[^{15}N]/[^{14}N]_{air\_N2}-1) \times 1,000‰$ and $\delta^{18}O = ([^{18}O]/[^{18}O]_{sample}/[^{18}O]/[^{16}O]_{VSMOW} - 1) \times 1,000‰]$. Based on replicate measurements of laboratory standards and samples, the analytical precision for NO_3^- $\delta^{15}N$ and $\delta^{18}O$ analyses was generally better than ±0.2 and ±0.3‰ (1 SD), respectively. For NO_2^- $\delta^{15}N$ and $\delta^{18}O$ analyses the analytical precision was ±0.4 and ±0.6‰ (1 SD), respectively.

Results

Hydro(geo)chemistry

A hydrochemical facies analysis of the karst aquifer (Fig. S1 of the electronic supplementary material (ESM)) reveals that most of the investigated groundwater can be classified as Ca^{2+}/Mg^{2+}-HCO_3^- type waters. As expected, the hydrochemical composition of the groundwater reflects the dissolution of the calcite and dolomite minerals dominating the aquifer matrix as has been reported for other carbonate aquifers (e.g., Einsiedl and Mayer 2005). Concentrations of Cl^- and SO_4^{2-} in the majority of groundwater samples were in the range of 0.1 to 0.65 mM and 0.1 to 0.94 mM, respectively. Both, the observed Cl^- concentrations and low molar Na^+/Cl^- ratios (Fig. S7 of the ESM) are common indicators supporting the anthropogenic origin of chloride in groundwater (e.g., Böhlke 2002). In contrast, sulfate can be expected to be predominantly of geogenic origin due to the presence of gypsum bearing formations overlying the Muschelkalk sediments. Two wells of Sulz am Eck (Sul3, Sul5) show elevated concentrations of Cl^- and particularly SO_4^{2-}, which is probably due to the admixture of water exposed to the underlying evaporite layers of the Middle Muschelkalk (e.g., Blanchette et al. 2010; Warren 2016), since the filter section of these wells starts just above these layers. A general summary of the average concentrations of the major and minor ions detected is shown in Table S1 of the ESM. CTD-based temperature measurements ranged from 10.0 to 11.0 °C (except Sul3, 12.0 °C). Overall, the temperatures are close to the mean annual temperature of the study area. Average values of specific electrical conductivity (SEC), pH and DO for the four different major sites are shown in Table 1. A circumneutral to slightly alkaline pH has been determined for all groundwater samples. Both, SEC and pH values fall within the range observed and commonly associated with karstified areas (Pronk et al. 2006; Ford and Williams 2007; Ravbar et al. 2011). Average DO concentrations at the field sites were usually close to saturation (except for ArtAlt), with occasionally concentrations significantly lower than 200 µM (Fig. S10 of the ESM). This implies that the groundwater is persistently influenced by oxic conditions in the recharge area and becomes anoxic under confined conditions at the location of the artesian well (ArtAlt).

Hydraulic and chemical groundwater response

Medium to large fluctuations in the hydraulic head (H) have been observed in most of the investigated wells, which is in accordance with findings from other karst aquifers (e.g., Ravbar 2013). Groundwater dynamics are presented in Fig. 2, including time series of daily precipitation, H and SEC during the period of Jan 2016 to Mar 2019. A direct comparison between H and daily precipitation indicates pronounced differences in

Table 1 Average values of specific electrical conductivity (SEC), pH and dissolved oxygen ±standard error for the four major sampling sites located within the Ammer catchment

Parameter/ Site	SEC [µS/cm]	pH	DO [mg/L]	Elevation [m asl]	GWT [m asl]
Sulz am Eck	754 ±77	7.3 ±0.1	6.4 ±0.1	528–588	490–515
Sul3[a]	1,187 ±134	7.2 ±0.1	7.3 ±0.1	511	490–497
Haslach	790 ±20	7.3 ±0.1	5.8 ±0.1	436–500	405–490
AMQ	925 ±12	7.3 ±0.1	8.7 ±0.5	403	403
ArtAlt	899 ±41	7.2 ±0.1	0.2 ±0.1	379	379–385

DO values are based on automatic probes (end of 2015 until 2016/2017), whereas SEC and pH has been determined during sampling campaigns (2004–2018). *AMQ* Ammer spring, *ArtAlt* Artesian well Altingen, *GWT* groundwater level (water table)

[a] Monitoring well No. 3 at Sulz am Eck: Values measured for Sul3 are presented separately because Sul3 is strongly influenced by additional evaporite dissolution which is also visible in particularly high SEC values

hydraulic responsivity of the individual wells towards precipitation events. The highest responsivity could be observed at Sul4 (Fig. 2a), where hydraulic heads increased within a few hours after rain events of about 10 mm or more, although amplitudes remained usually small (for details see Fig. S2 of the ESM). The lowest responsivity (but at highest amplitudes) was observed at Has5 (Fig. 2b), which seemed responsive to very strong precipitation events only, primarily during the recharge period in the winter season when evapotranspiration is low. In the majority of the wells, water-table reactions after rain events of at least 20 mm occurred within 1 or 2 days; however, extended but lower intensity rain events sufficed to trigger a hydraulic response during the winter season.

All groundwater wells, except Has5, show a clear reaction of SEC to rain events (Fig. 2) within 1–4 days after the events, which suggests that the observed increase in H was at least partly governed by inflow of a different water component, and not solely a pressure response. At Has2 and Sul1, the SEC response (i.e., dilution peaks) happened nearly synchronous with the rise in hydraulic heads, followed by slightly delayed (2–10 days) but fast increases in SEC. SEC dilution

dominated at Sul4, where almost all hydraulic responses were accompanied by a small decrease of SEC. The 10–60% increase in SEC after rain events at Sul1, Has2, and Has4 indicates a contribution of a water component with higher mineralization than under baseflow conditions. A similar increase in SEC was observed at Has2 after a strong rain event in Mar 2020 (25 mm within 1 day), which was accompanied by increases of about 10–20% in the concentrations of Na^+, Ca^{2+}, Mg^{2+}, and Cl^-, respectively (see Table S2 of the ESM). The much higher variability of SEC at Sul3 is most likely related to the more saline groundwater component from the Middle Muschelkalk, which is strongly diluted after rain events. Overall, the combined hydraulic and chemical responses observed suggest that at least two water components are mobilized during stronger rain events, which reach the groundwater wells within a few days.

Spatial and temporal variability in nitrate concentrations

NO_3^- concentrations detected in the studied groundwaters (except ArtAlt) were comparatively high, with median values between 0.10 and 0.84 mM (6–52 mg/L)
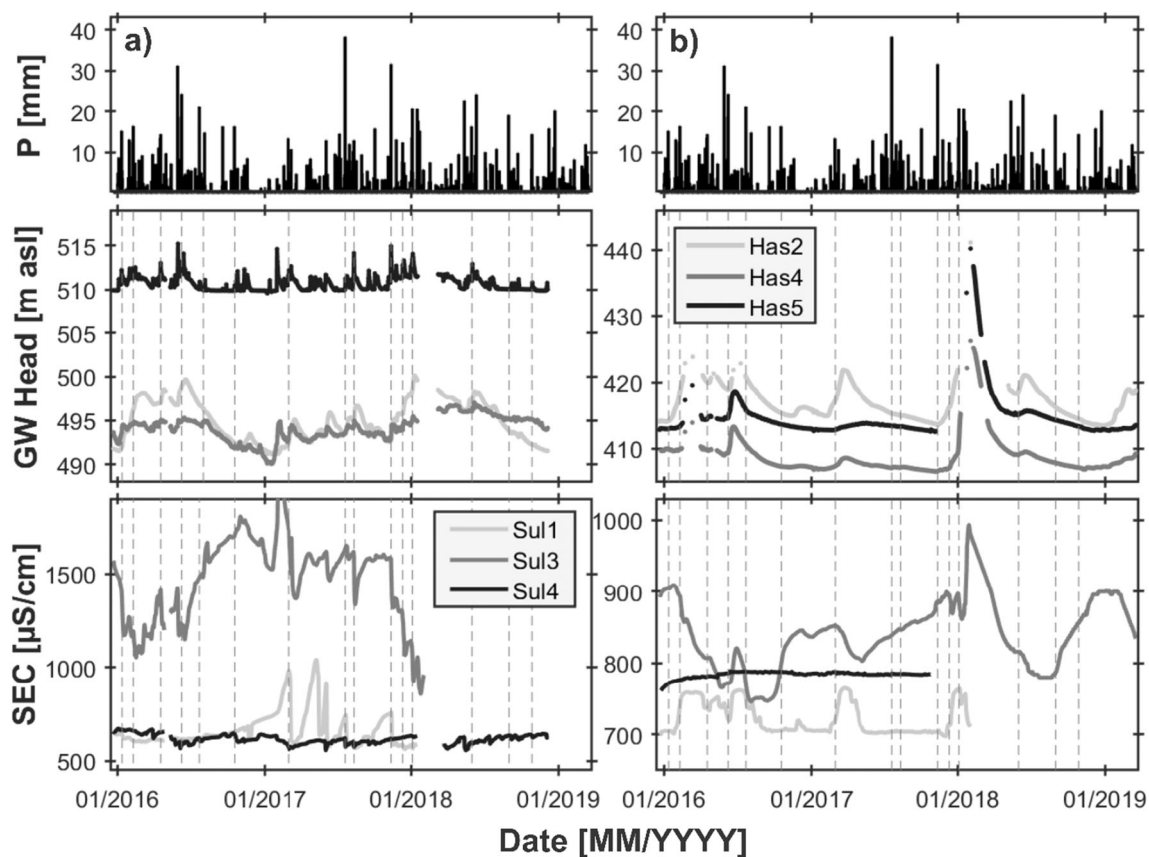

Fig. 2 Time series of precipitation (P), hydraulic head (H) and specific electrical conductivity (SEC) at **a** Sulz am Eck and **b** Haslach for the period Jan 2016 to Jan 2019. Dashed grey lines (perpendicular to x-axis) indicate precipitation events larger 20 mm within less than or equal to 2 days. Note that P (**a**–**b**) is identical since the data depicted here were taken from the Bondorf station (Haber and Hintemann 2019). Single graphs are provided in addition in Fig. S2 of the ESM

(Fig. 3; Fig. S2 of the ESM). The highest NO_3^- concentration, which even exceeded the NO_3^- concentration that are admissible under the German Drinking Water Ordinance (50 mg/L), was detected at Has5. At the same time, a pronounced spatial variability in NO_3^- concentrations between the individual wells was observed at Sulz am Eck and Haslach (Fig. 3). The median NO_3^- concentrations of the four major field sites show an apparent increase from Sulz am Eck towards Haslach and the AMQ (Fig. 3). By contrast, NO_3^- concentrations were relatively low or undetectable (<0.002 mM) at ArtAlt.

In contrast to the pronounced spatial variability at Sulz am Eck and Haslach, seasonal NO_3^- concentration fluctuations appear to be minor (see Fig. 4; Fig. S3 of the ESM). Only at AMQ did the NO_3^- concentrations show subtle fluctuations throughout the year, peaking during winter and early spring. There are no clear NO_3^- variations discernible at the wells of Sulz am Eck and Haslach. NO_3^- concentrations detected at ArtAlt throughout the years (2010–2018) remained steady at relatively low values around 0.02 mM (1.3 mg/L).

Nitrite concentrations in groundwater

NO_2^- was analysed in samples taken from selected wells during the sampling campaigns in Apr 2016 and Jan 2018. NO_2^- concentrations were high in Apr 2016 (except at ArtAlt), ranging from 0.05 to 0.14 mM (Fig. S4 of the ESM); however, the observed NO_2^- concentrations did not show any clear relation with NO_3^- concentrations. Although similar NO_3^-

concentrations (0.15 to 0.73 mM) were found for the sampling campaign in Jan 2018, NO_2^- was close to, or below, the detection limit of about 0.0002 mM in all wells. While low concentrations of NO_3^- were detected at ArtAlt during both sampling campaigns (0.04–0.07 mM), NO_2^- was neither detected during Apr 2016 nor Jan 2018.

Nitrate and nitrite stable isotopes

Dual isotope ratios ($\delta^{15}N$- and $\delta^{18}O$) of NO_3^- and NO_2^- were measured in April 2016 in order to gain additional insights into the potential origins of NO_3^- (Fig. 5). The NO_3^- $\delta^{15}N$ values ranged from ~+8 to +25‰ (Fig. 5a), whereas $\delta^{18}O$-NO_3^- values ranged between 0 and +20‰ (Fig. 5b). Only Sul3 showed higher values for both $\delta^{15}N$- (+31‰) and $\delta^{18}O$-NO_3^- (+37‰). The lowest NO_3^- concentrations were measured at ArtAlt; however, $\delta^{15}N$- and $\delta^{18}O$-NO_3^- values fall within a similar range as observed in the other wells. Except for the comparatively high values determined in Sul3 waters (possibly indicating partial denitrification), NO_3^- $\delta^{15}N$- and $\delta^{18}O$ fall within a range typically associated with the application of either mineral fertilizers or manure as sources of N (see Table S3 of the ESM). However, based on the somewhat intermediate NO_3^- $\delta^{15}N$ values at all sites except Sul3, distinguishing between these two sources (i.e., nitrification of either artificial fertilizer or manure-derived N compounds) is problematic.

NO_2^- concentrations were high enough for NO_2^- $\delta^{15}N$ and $\delta^{18}O$ measurements in samples taken in April 2016 (Fig. 6). $\delta^{15}N$-NO_2^- values vary widely between the wells and range from roughly −9 to +20‰ (Fig. 6a). The NO_2^- $\delta^{15}N$ values
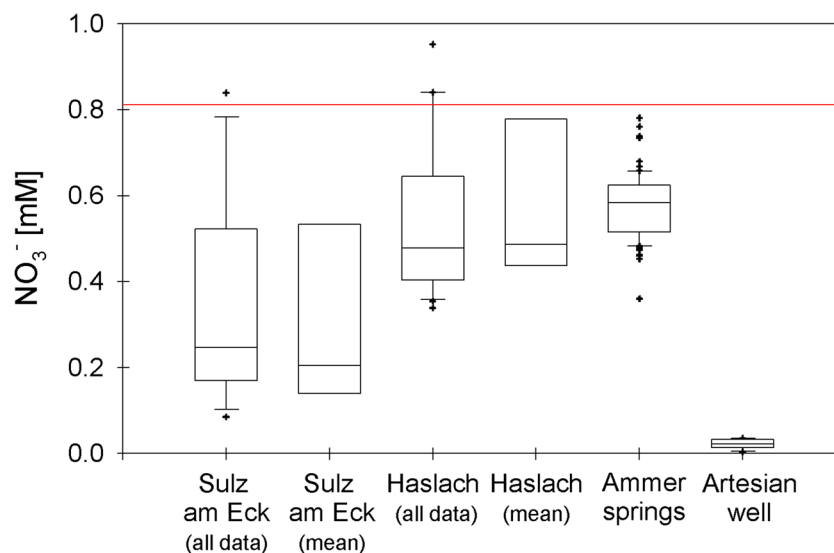

Fig. 3 Box and whisker plot of nitrate concentrations for the years 2010 to 2018. For Sulz am Eck and Haslach two box plots are shown, the first based on all nitrate measurements over the given time period (all data), the second averaging NO_3^- concentrations for the individual wells over time (mean). The consistent distribution of both data sets indicates that NO_3^- concentrations are dominated by spatial variability. The end of the whiskers marks the outliers, whereas the median is depicted as the black line within the box. The red line marks the threshold value of 50 mg/L (0.806 mM) NO_3^- in drinking water as defined by the European Union as the maximum statutory limit (ECETOC 1988)

Fig. 4 Time series of nitrate concentrations detected at the different field sites from 2005 to 2018. **a** Ammer spring AMQ and the artesian well Altingen, ArtAlt are presented for comparison. Nitrate concentrations of **b** Sulz am Eck and **c** Haslach are presented separately
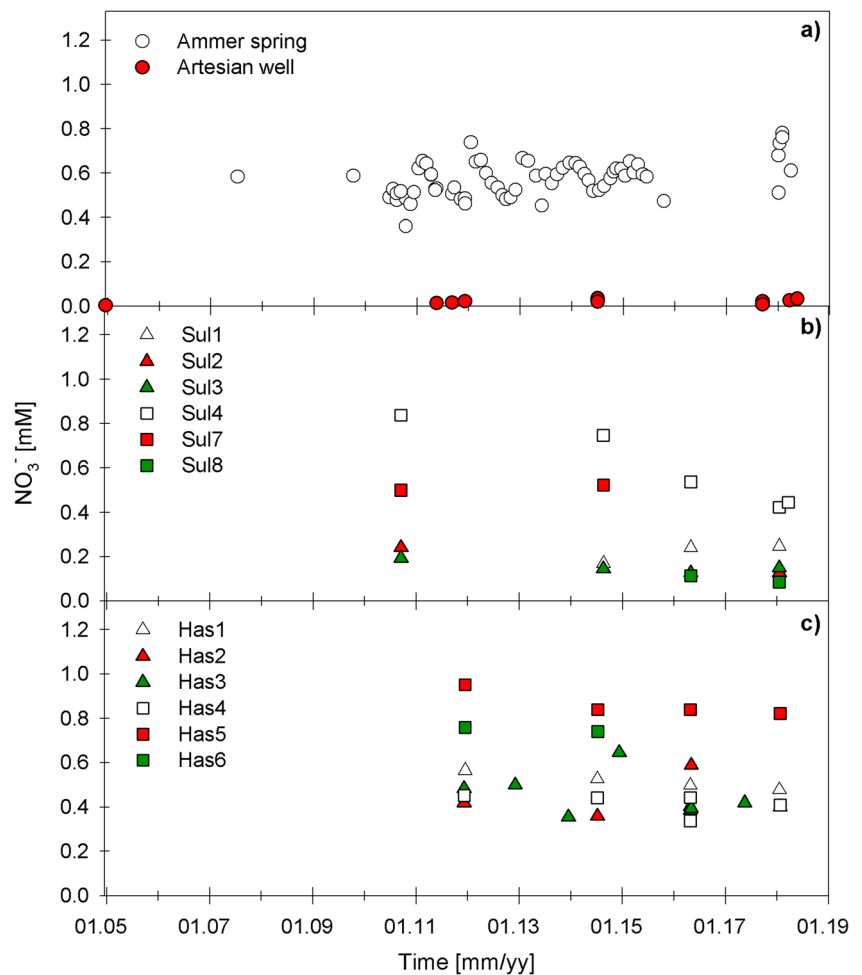
are always lower than their corresponding NO_3^- $\delta^{15}N$ values (Fig. 5 vs. Fig. 6, note the different scales), and therefore possibly suggest ongoing denitrification. The highest $\delta^{15}N$-NO_2^- value (+20‰) is observed at Sul3, which also has the highest $\delta^{15}N$-NO_3^- value (+31‰). The measured $\delta^{18}O$-NO_2^-

values vary only slightly between the wells within a range of +2 to +6‰ (Fig. 6b). Again, $\delta^{18}O$-NO_2^- values (Fig. 6b) are systematically lower than the corresponding $\delta^{18}O$-NO_3^- values (Fig. 5b); yet, a possible impact by oxygen atom exchange affecting the $\delta^{18}O$-NO_2^- values, either during NO_2^-

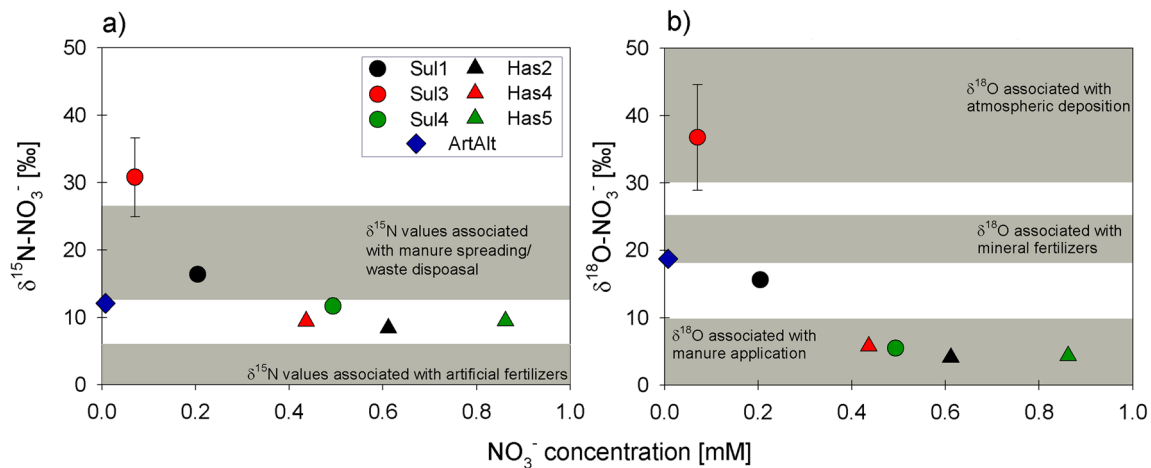**Fig. 5** Nitrate **a** $\delta^{15}N$ and **b** $\delta^{18}O$ values plotted against the NO_3^- concentrations detected in selected groundwater wells at Sulz am Eck and Haslach in Apr 2016. Marked areas illustrate typical isotopic ranges of various nitrate sources as reported in previous studies (for details see Table S3 of the ESM). Standard deviation for technical replicates represented by error bars

Fig. 6 **a** δ^{15}N- and **b** δ^{18}O-NO$_2^-$ values plotted over NO$_2^-$ concentrations detected in selected groundwater wells at Sulz am Eck and Haslach in Apr 2016. Error bars represent the standard deviation calculated from technical replicates (CF-IRMS). Note that, for δ-values, different scales are applied
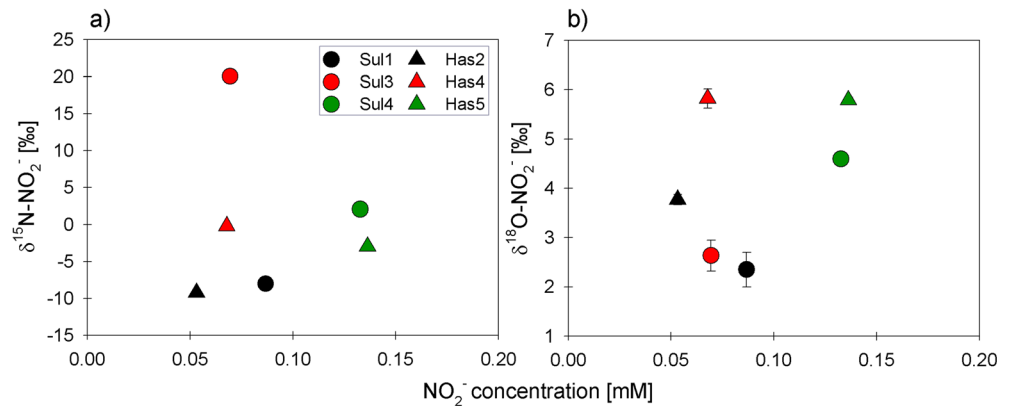
production/accumulation and fractional denitrification within the groundwater, or due to method-inherent O-isotope exchange during storage and/or analysis with the azide method, cannot be excluded.

Land use in the well capture zones

Groundwater capture zone delineation was used to evaluate the potential agricultural impact on NO$_3^-$ concentrations at the single wells. Capture zones of all wells located at the two major field sites Sulz am Eck and Haslach were delineated by backward particle tracking, using a recently established groundwater flow model of the Muschelkalk aquifer (D'Affonseca et al. 2020). All capture zones followed the general groundwater flow direction across forested and arable land (Fig. 7). While groundwater flow at Sulz is mainly controlled by the aquifer dipping direction (ESE), the flow regime at Haslach is increasingly influenced by the Ammer springs, causing the trajectories of the Haslach wells to be more SSE oriented; therefore, the length of the capture zones ranged from <0.5 km (Sul4, Sul7) to ~6 km (Has3, Has4).

Based on these delineations, the capture zone area (ha) was estimated for the major land use categories using aerial images of the study period (Fig. S5 of the ESM). Overall, wells at both field sites appear to be dominated by water deriving from agricultural land. Proportions (%) of the main land use categories associated to each well are shown in Fig. S6 of the ESM. Wells such as Sul1, Sul2a and Has5 are instead proportionally more affected by forested areas.

Discussion

The groundwater in the recharge area of the karst aquifer displayed a relatively large spatial variability of NO$_3^-$ concentrations, exceeding the temporal variations at individual sites in most cases (see Fig. 3). In the sections that follow, deeper insight into the hydrogeological and biogeochemical processes that govern the observed NO$_3^-$ variability, both from a

hydrochemical as well as from an isotopic-tracer perspective, are provided. The complementary information provided by monitoring wells connected to different portions of the heterogeneous flow system, as compared to karstic springs, allow in turn the refinement of the conceptual models of N transport in the karst aquifer.

Nitrogen sources and nitrate variability

Since arable land comprises a large proportion of land use in the recharge area, most groundwater NO$_3^-$ can be expected to originate from agricultural practices (Einsiedl and Mayer 2006; Gurdak and Qi 2012). Other potential anthropogenic N sources in the study area include septic systems of isolated houses and workshops. However, a screening of typically sewage-derived organic micro-contaminants (i.e., carbamazepine, clofibric acid, metoprolol, sulfamethoxazole; e.g., Heberer 2002; Whelehan et al. 2010) in the study area did not show concentrations above 1 ng/L for any of these substances, suggesting that N-compound contamination associated with wastewater is negligible. Inorganic constituents derived from agricultural additives such as Cl$^-$ or SEC, are commonly considered useful indicators for agriculturally derived NO$_3^-$ inputs in groundwater (Böhlke 2002; Boy-Roura et al. 2013). The Na$^+$/Cl$^-$ molar ratios of <1 (Fig. S7 of the ESM) indicate that Cl$^-$ mainly derived from sources other than NaCl such as KCl, which is commonly applied as artificial fertilizer (Böhlke 2002). Analysis of dissolved Cl$^-$ and NO$_3^-$ concentrations performed for all four field sites revealed a positive correlation of the two solutes at Sulz and Haslach (Fig. 8), supporting the influence of agriculture on NO$_3^-$ concentrations. A different pattern was found for AMQ, where no clear relationship between NO$_3^-$ and Cl$^-$ was discernible, and a regression analysis even yielded a negative slope (Fig. 8c). However, NO$_3^-$ concentrations at AMQ showed a positive trend with elevated discharge, whereas Cl$^-$ was diluted at higher discharge (Fig. S8 of the ESM). Such opposing relations are usually observed when discharge is controlled by rapid infiltration and transport of event water through
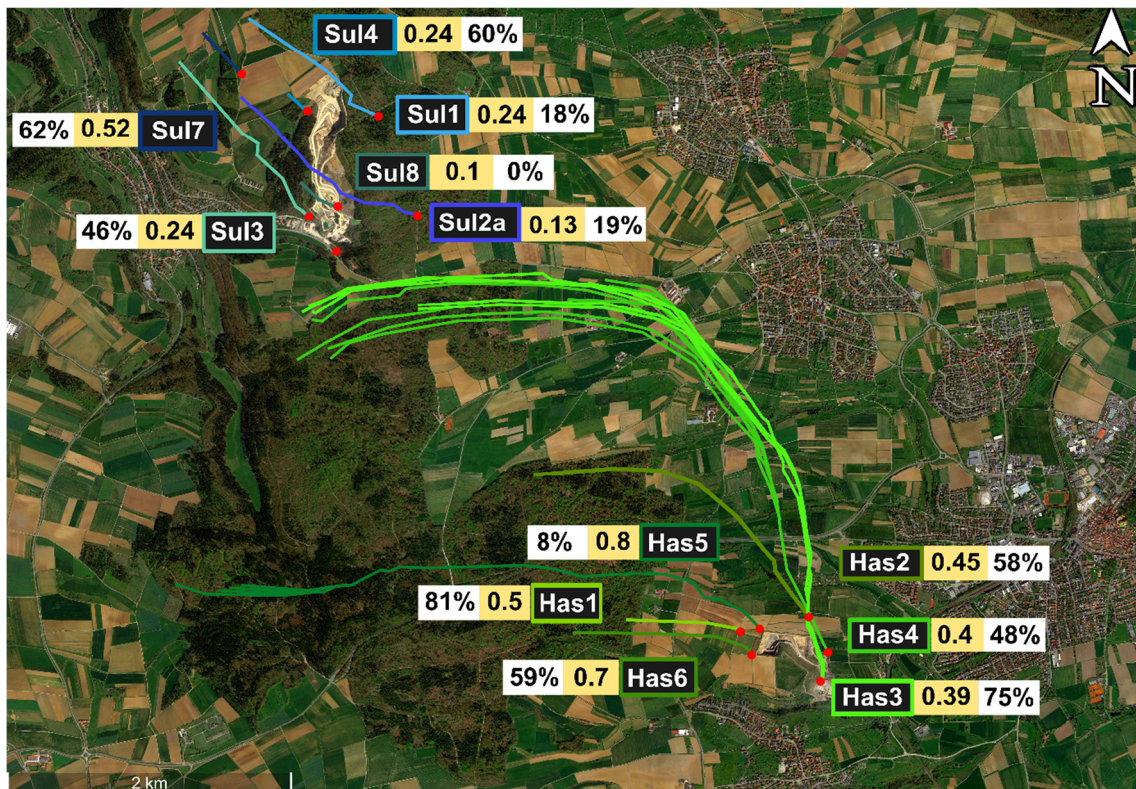
Fig. 7 Delineation of the well capture zones based on reversed particle tracking. Red dots mark the well locations at the field sites Sulz am Eck and Haslach. Boxes contain the well ID, nitrate concentration in mM (light yellow) and the estimate of arable land within the well capture zone in percent (white). Lines of well capture zones are colour-coded. The image was taken from Google Earth, 2019 and adapted by using maps provided by LUBW (LUBW Landesanstalt für Umwelt 2017)

Fig. 8 NO_3^- versus Cl^- plots for **a** monitoring wells at Sulz am Eck, **b** monitoring wells at Haslach, **c** the karstic spring AMQ, and **d** the artesian well ArtAlt. Values of well Sul3 are located outside the used axis scale as indicated by the arrow. Trend lines (**a–b**) do not include outliers with low NO_3^-/Cl^- ratios. For comparison, the trend lines (**a–b**) are again shown (**d**). The given NO_3^-/Cl^- ratios are valid for samples near the trend lines (where applicable) or the centre of the data cluster for AMQ, where a clear correlation could not be discerned
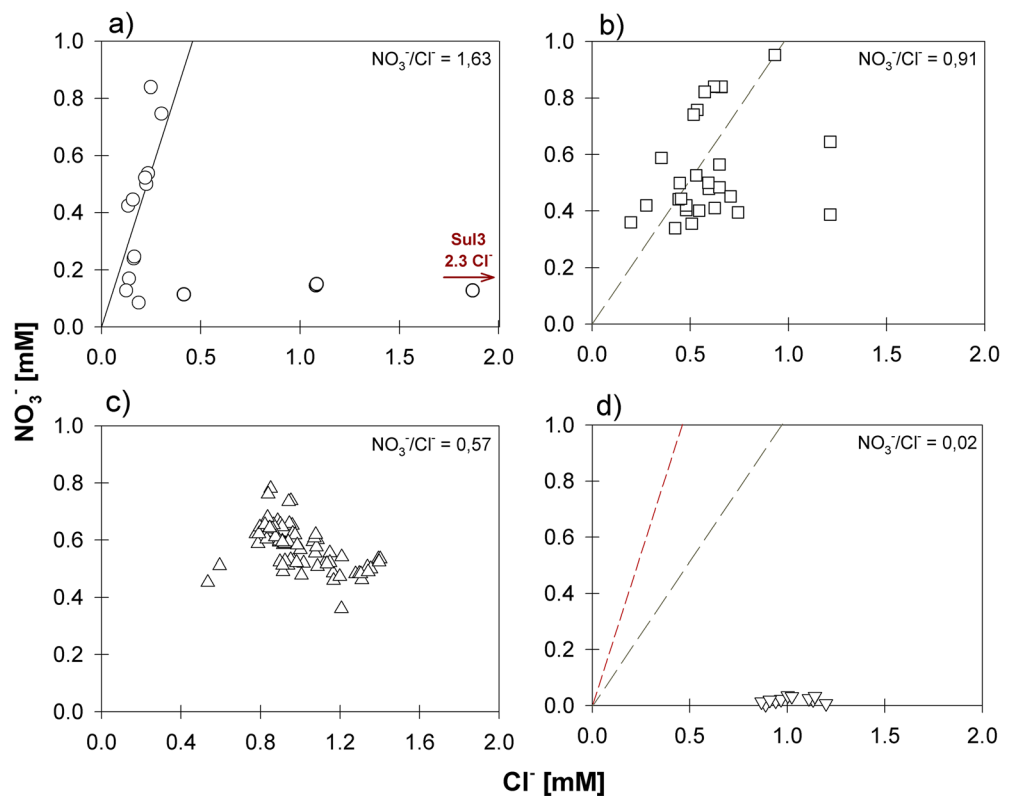
agricultural soils and connected karst conduits (Musgrove et al. 2016; Asante et al. 2018; Husic et al. 2019).

The NO_3^- isotope values detected in the groundwater from Sulz am Eck, Haslach and ArtAlt lend further support to agriculture-derived fertilizer N as the main source of NO_3^- (Fig. 5; typical value ranges are summarized in Table S3 of the ESM). The $\delta^{15}N$-NO_3^- values ranged from +9 to +31‰ (Fig. 5), suggesting that manure spreading and/or artificial fertilizer applications are the main source of NO_3^- (Kendall et al. 2007; Nikolenko et al. 2018). Volatilization during storage, treatment and application of manure (NH_3) often results in a significant ^{15}N enrichment of the remaining NH_4^+ pool, and thus NO_3^- produced via nitrification commonly yields high $\delta^{15}N$ values up to +35‰ (Kendall and Doctor 2005; Nikolenko et al. 2018). NO_3^- from naturally soil-derived, organically bound N with $\delta^{15}N$ values ranging from −10 to +15‰ (Kendall et al. 2007) might act as an additional source but can only explain isotope values observed in a few low-concentrated samples. Forested areas have been reported to be characterized not only by lower overall NO_3^- concentrations but also by comparatively low $\delta^{15}N$-NO_3^- values (<5‰) (Schwarz et al. 2011). Considering the delineation of the well capture zones, $\delta^{15}N$-NO_3^- values could, therefore, be additionally influenced by processes occurring in the area below forested and arable soils. Highest $\delta^{15}N$- (~+31‰) and $\delta^{18}O$-NO_3^- (~+38‰) values were detected at Sul3 indicating possible influences from isotope fractionation occurring during denitrification. The enriched $\delta^{18}O$-NO_3^- values may also be a result of NO_3^- from atmospheric deposition (Yue et al. 2017; Nikolenko et al. 2018), which bypassed the organic soil-N pool during infiltration of rain water through larger karstic structures. However, SEC data show that water mobilized during rain events towards the monitoring wells comprises only a small fraction of a quick flow component. Therefore, it seems unlikely that NO_3^- from atmospheric deposition reaches the monitoring wells undiluted and without further (bio-) geochemical processing.

Impact of land use on nitrate concentrations

Agricultural land use has been generally recognized as the major control of NO_3^- concentrations in groundwater (Nolan and Stoner 2000; Gurdak and Qi 2012). At the study sites, a corresponding trend is indicated by increasing NO_3^- contents with a larger proportion [fraction, %] of agricultural land use (arable land and intensive grassland) in the capture zone of the wells (Fig. 9). However, for wells with NO_3^- concentrations above 0.4 mM (~25 mg/L) the link between NO_3^- and fraction of agricultural land use becomes less clear, which might be partly due to the only rudimentary knowledge of the locations of hydraulically active fractures or karst conduits, which inevitably also limits the exactness of the simulations of the groundwater flow model (D'Affonseca et al. 2020). Though
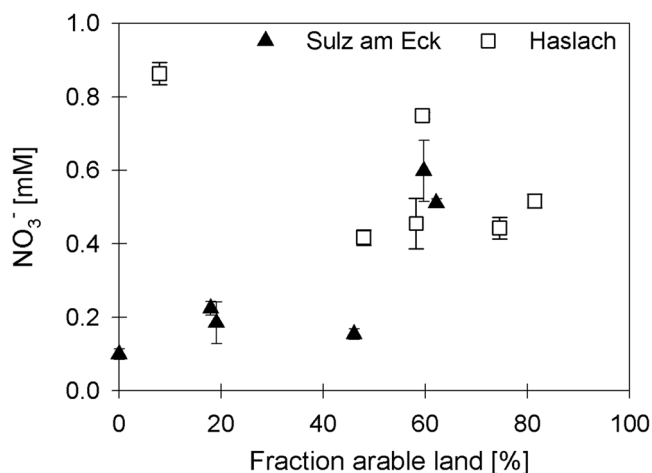

Fig. 9 Correlation between average NO_3^- concentrations and fraction [%] of arable land (arable land and intensive grassland) for both Sulz am Eck and Haslach. Error bars represent the standard error

the modelled capture zones might not accurately represent their actual positions, the resulting uncertainties in land use category remain acceptable, because of the uniform land use patterns along the general groundwater flow direction. A more severe effect on land use may be introduced by the presence of unmapped, i.e., soil-covered or not fully developed, karstic underground structures such as dolines or swallow holes, commonly promoting point-infiltration and percolation of surface-derived waters into karst conduits (Goldscheider 2005; Sauter et al. 2006; Ravbar and Goldscheider 2009). At these structures, enhanced infiltration of water and NO_3^- can be expected (rather than an even distribution within the capture zone), contributing to the observed spatial variability in NO_3^- concentrations. Depending on the location of the karstic structure in forests or below arable fields, this may lead either to a dilution or concentration of NO_3^-. Although the positive trend between Cl^- and NO_3^-, as well as $\delta^{15}N$-NO_3^- values, of the different wells suggest that agricultural N inputs massively contribute to the overall NO_3^- loading of the studied groundwater, other more local processes appear to affect spatial variability (Fig. 7) additionally, and in some instances to a greater extent.

Nitrate transport to the water table

Various conceptual models describing contaminant (NO_3^-) transport in karstified aquifers have been proposed in previous studies (Einsiedl et al. 2005; Bakalowicz 2005; Hartmann et al. 2014). The conceptual model presented here (Fig. 10) differentiates between flow and transport towards groundwater monitoring wells at two distinct locations with respect to the fracture and conduit network, and karstic springs directly connected to karst conduits. Flow within the fractured aquifer is usually characterized by a broad distribution of flow paths ranging from quick or shaft flow (in conduits, joints, or larger
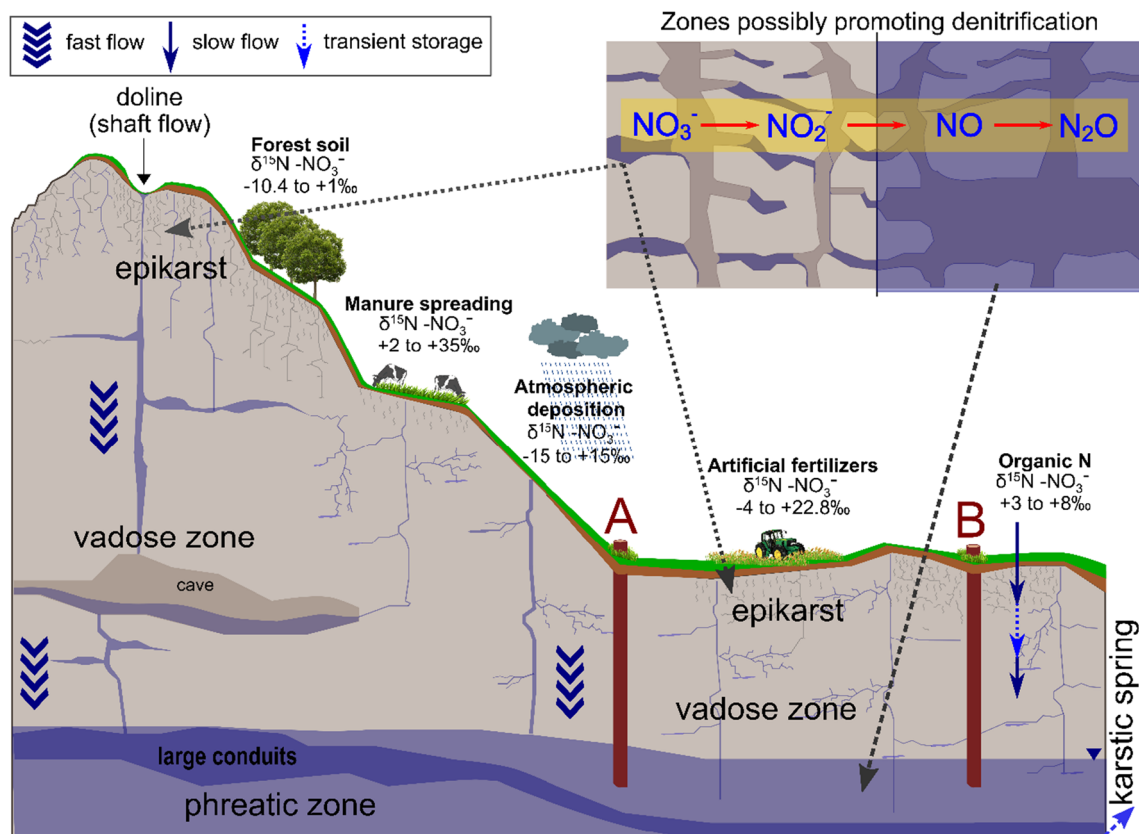
Fig. 10 Conceptual model of potential nitrate sources, transport, and turnover in the recharge area of karstic aquifers. Wells close to major conduits (A) can be expected to respond to nearly all major rain events (though at low amplitude). In contrast, wells influenced by waters deriving from the fracture and fissure system (B) will show lower responsivities yet with higher amplitudes due to the low porosity of the carbonic rocks. Zones promoting denitrification are possibly present in oxygen-depleted niches located within the epikarst or the fissure/matrix network of the phreatic zone. Isotope values are based on Nikolenko et al. 2018

fractures), via intermediate flow (due to displacement of transiently stored water in the epikarst or phreatic zone), to slow diffuse flow (in fissures or the pore matrix) (Perrin et al. 2003; Einsiedl 2005; Page et al. 2017). The epikarst comprises the near-surface weathering zone of the carbonate rocks immediately below the soil and consists of fractures and joints widened by dissolution (Ford and Williams 2007; Medici et al. 2019). How exactly N compounds are transported by infiltrating water towards, and below, the water table (e.g., the transport paths indicated in Fig. 10) can be expected to also influence NO_3^- concentrations in groundwater (Husic et al. 2019). The combined hydraulic and chemical response observed at the study site suggested that at least two water components are mobilized during stronger rain events, reaching the groundwater monitoring wells within a few days. Evidence for the contribution of quick flow infiltrating the karst system along shafts and larger fractures is provided by the observed SEC dilution peaks occurring nearly simultaneously (<1 day) with major rain events in Sul1, Sul4 and Has2. This is further supported by the hydraulic head response at these wells, showing high responsivity yet with only moderate amplitudes, which might best be explained by the close proximity to large-volume karst structures (Ford and Williams 2007; Medici et al. 2019) (see well A, Fig. 10). However, the response of hydraulic heads is not necessarily caused by water fluxes at the well locations and hence, in contrast to spring hydrographs, cannot be used to separate flow components directly.

In some of the wells, the hydraulic-head response was accompanied with distinct subsequent increase in SEC, indicating the mobilization of a water component with higher mineralization within only a few days. Similar increases in SEC observed at karstic springs have frequently been attributed to pulses of water from the subcutaneous or epikarst zone (Williams 1983; Lakey and Krothe 1996; Ravbar et al. 2011). The displacement of water stored temporarily in the epikarst or other compartments by large rain events is therefore a plausible cause explaining the SEC variations. This is supported by the increase in Ca^{2+} and Mg^{2+} concentrations observed after a strong rain event in Has2 (Table S2 of the ESM). In Fig. 10, such a scenario would correspond to the transport path to well B. Due to a decreasing permeability with depth towards the unweathered and less karstified bedrock, the epikarst is known to act as transient storage of infiltrating

water (Jones 2003; Fidelibus et al. 2017). The resulting longer residence times, as well as high CO_2 and organic carbon contents in the nearby soil, not only promote carbonate dissolution but possibly may also cause transient O_2 deficiency and in fractional N turnover (Fidelibus et al. 2017). Besides the epikarst, transient storage could also be induced by diffusive exchange between the rock matrix and small fractures and fissures in the phreatic zone. These at least transiently water-saturated zones might also develop the potential to promote organotrophic denitrification, e.g., in anoxic niches (Husic et al. 2019), although the overall contribution to the spatial variability of NO_3^- may be limited. Given the relatively large increase of SEC after rain events, as compared to dilution of SEC, the groundwater wells in the recharge area of the karst aquifer appear to be predominantly influenced by water from transient storage rather than by quick flow.

In contrast to the monitoring wells of Sulz am Eck and Haslach, former tracer tests gave clear evidence that the AMQ is directly connected to the karstic conduit system (Harreß 1973). Hence, the steady NO_3^- levels at AMQ represent an average value integrating over the catchment's different water flow paths and storage compartments drained by the conduit system. NO_3^- originating from the near soil surface is considered to dominate recharging water since it is mobilized by intense rainfalls resulting in high NO_3^- but low Cl^- concentrations during peak discharge of the spring (Huebsch et al. 2014).

Evidence for N turnover

In general, karstified aquifers and particularly karstic springs are known to contain oxygen-rich waters (Kendall and Doctor 2005; Ford and Williams 2007; Benk et al. 2019). DO concentrations above 200 nM have been shown to impact denitrification-related gene expression (Dalsgaard et al. 2014) and concentrations above 5 μM has traditionally been assumed to inhibit denitrification (Codispoti et al. 2001); therefore, the vadose zone and the epikarst are generally considered as storage compartments for NO_3^-, and a zone of nitrification rather than denitrification (Einsiedl et al. 2005; Fidelibus et al. 2017; Ascott et al. 2017). However, previous findings on the O_2 sensitivity of denitrifying enzymes have partially been revised (Takaya et al. 2003; Schreiber et al. 2012; Kuypers et al. 2018) and various microorganisms have been shown to successfully perform dissimilatory NO_3^- reduction to NO_2^- also under hypoxic and even oxic conditions (Roco et al. 2016; Zhou et al. 2019; Cojean et al. 2019). This is in accordance with studies providing evidence for ongoing denitrification within the vadose and/or epikarst zone (Brahana et al. 2005; Kuniansky and Spangler 2014; Panno et al. 2001), as well as at oxic and anoxic groundwater monitoring wells of a limestone aquifer (Henson et al. 2017; Wegner et al. 2018). The data from this study support these

previous findings, suggesting the presence of microooxic to anoxic niches located within the epikarst (close to the organic rich soil) and/or the phreatic zone (omnipresent Fe(II)-bearing carbonates). Some of the investigated wells show large temporal changes of dissolved oxygen concentration, with minimum DO values < ~51 μM at Sul1 (Fig. S10 of the ESM). The low DO concentrations in Sul1 and other wells (see Table 1) indicate that parts of the water in these wells, at least temporarily, undergo enhanced oxygen consumption. While O_2 respiration obviously does not lead to complete O_2 consumption and anoxia in the major conduits, it is reasonable to hypothesize that suboxic and even anoxic conditions can occur locally, providing important microenvironments for denitrification in waters already relatively low in O_2.

In order to elucidate possible N turnover processes, $\delta^{15}N$- and $\delta^{18}O$-NO_3^- values versus molar NO_3^- concentrations are plotted on an antiproportional (Keeling plot) and a logarithmic scale (Rayleigh plot) (Fig. 11a,b, after Kendall and Doctor 2005). A fractionating process like denitrification would lead to an exponential relationship, and plotting $\delta^{15}N$- and $\delta^{18}O$-NO_3^- values versus the natural logarithm of the NO_3^- concentrations will produce a straight line. If an exponential relation is not observed and a straight line is produced on a Keeling plot, the NO_3^- concentration and isotope composition trends are governed by simple mixing of two endmembers. The available data trends are explained equally well by the two regression models, suggesting that the two processes (mixing with a high-δ N source and fractionation during denitrification) cannot be clearly distinguished at the investigated sites. Mixing of water and NO_3^- from different sources is the natural result of sample collection by extracting groundwater from extended well screens, thus including contributions from different groundwater flow paths.

However, the presence of N turnover processes in the groundwater system is clearly indicated by NO_2^- concentrations of up to 0.14 mM (see Fig. S4 of the ESM), which were observed in wells at Sulz am Eck and Haslach during the sampling campaign in Apr 2016. NO_2^-, a highly reactive intermediate, is commonly produced enzymatically either during nitrification or denitrification (Knowles 1982; Kendall and Aravena 2000; Zhu et al. 2013). Taking into account the difference between the $\delta^{15}N$ values of NO_3^- and NO_2^- (defined as $\Delta\delta^{15}N = \delta^{15}N\text{-}NO_3^- - \delta^{15}N\text{-}NO_2^-$), the $\delta^{15}N\text{-}NO_2^-$ data appear to be consistent with denitrification as the dominant NO_2^- source, rather than nitrification. The $\Delta\delta^{15}N$ values were consistently positive, ranging between 9.6 ± 0.4‰ and 24.4 ± 0.5‰ (i.e., all $\delta^{15}N\text{-}NO_2^-$ values were lower than the corresponding $\delta^{15}N\text{-}NO_3^-$ values), but not large enough to be solely explained by ongoing nitrification. Nitrification is a two-step microbially mediated process, where ammonium (NH_4^+) is first oxidized via the intermediate hydroxylamine (NH_2OH) to NO_2^-, which is subsequently further oxidized to NO_3^- (e.g., Casciotti 2009). Isotope fractionation during NH_4^+ oxidation

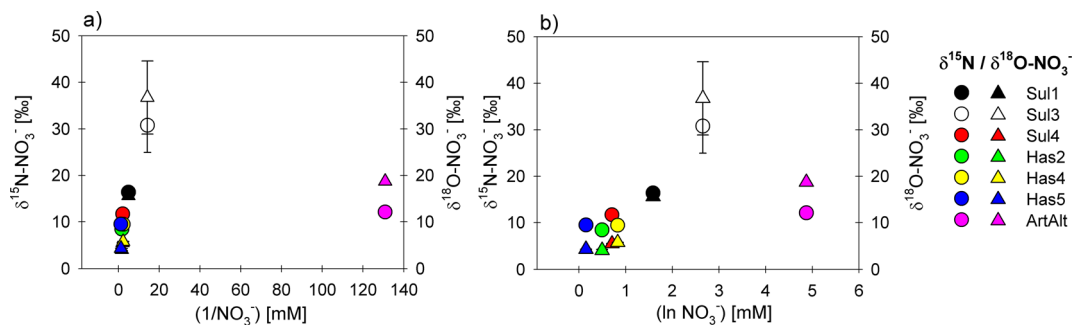**Fig. 11** Analysing δ^{15}N- (circles) and δ^{18}O- (triangles) NO$_3^-$ values for **a** source mixing using a Keeling plot and **b** denitrification using a Rayleigh plot. Standard deviation from technical replicates for CF-IRMS measurement is included as error bars ($n = 2$). ArtAlt, which is commonly anoxic, is added for comparison

leads to the enrichment of heavy ^{15}N in the remaining NH$_4^+$ pool (resulting enrichment factor ranging from +14 to +38‰) and produces isotopically lighter NO$_2^-$ (e.g., Casciotti 2009). The second step, the oxidation of NO$_2^-$ to NO$_3^-$, however, results in an inverse isotope effect, where the product (i.e., NO$_3^-$) instead of the residual NO$_2^-$ gets enriched in heavy ^{15}N (resulting enrichment factor −12.8‰; Casciotti 2009). Therefore, isotope fractionation during nitrification would result in rather low (<−30‰) δ^{15}N-NO$_2^-$ values (Casciotti 2009). In contrast, isotope fractionation during denitrification — the stepwise reduction of NO$_3^-$ via NO$_2^-$, nitric oxide (NO), nitrous oxide (N$_2$O) to gaseous N$_2$— is characterized by individual enrichment factors for each reduction step (NO$_3^-$ reduction: +5 to +30‰; NO$_2^-$ reduction: +5 to +25‰; N$_2$O reduction: +4 to +13‰), resulting in the enrichment of ^{15}N in the respective substrate pools (e.g., Granger et al. 2008; Casciotti 2009). Hence, denitrification is expected to result in δ^{15}N-NO$_2^-$ values that are roughly 0–30‰ lighter than the δ^{15}N of the residual NO$_3^-$. If denitrification is incomplete or partially inhibited by, e.g., hypoxic O$_2$ levels, nitrification might occur, leading to even lower δ^{15}N-NO$_2^-$ values and thus larger $\Delta\delta^{15}$N (Casciotti 2009; Bourbonnais et al. 2015). Wells et al. (2016) suggested a $\Delta\delta^{15}$N value of ~50‰ as clear indication for coupled denitrification and nitrification in a groundwater system, substantially larger than the $\Delta\delta^{15}$N values observed at groundwater sites in this study.

Hence, the observed positive but relatively small difference in δ^{15}N between the NO$_2^-$ and the remaining NO$_3^-$, in combination with the relatively high NO$_3^-$ δ^{15}N- and δ^{18}O values and low NO$_3^-$/Cl$^-$ ratios in some of the wells (e.g., Sul3) provide putative evidence for microbial denitrification despite DO levels that do not indicate prevailing anoxic conditions within the system. At the same time, it should be noted that groundwater denitrification, particularly if it occurs in micro niches, does not necessarily lead to elevated NO$_3^-$ δ^{15}N- and δ^{18}O values. More precisely, the biological N (and O) isotope effects of denitrification could possibly be masked not only by the mixing of waters emerging from different flow paths but also by NO$_3^-$ transport limitation and in turn complete

substrate consumption within the actively denitrifying microenvironments (Brandes and Devol 1997). Hence, microbial denitrification may not be restricted to Sul3 only, where the highest NO$_3^-$ N and O isotope values were observed.

Although the results indicate that denitrification is ongoing in the aquifer, there is no clear evidence on which electron donor is involved in NO$_3^-$ reduction. Organic matter, due to proximity to soils, may be important in the epikarst; however, DOC concentrations were generally relatively low (<0.3 mM; Fig. S12 of the ESM), and no correlation was observed between NO$_3^-$ and DOC concentrations (Fig. S13 of the ESM), suggesting that metabolic pathways other than organotrophic denitrification might play a role, e.g., involving Fe(II)-bearing minerals (Wegner et al. 2018; Schwab et al. 2019) such as pyrite (up to several weight% in the Muschelkalk). In light of the overall high sulfate concentrations at the studied sites (0.8 mM; due to the dissolution of gypsum), it is impossible to detect the production of sulfate via sulphide-dependent denitrification (via its anti-correlation with NO$_3^-$), even if rates were quite high (Fig. S14 of the ESM). Dissolved Fe^{2+} concentrations were usually below 0.02 mM, but reached significantly higher levels at least at Has5 and Sul3 (0.03 and 0.4 mM, respectively; Fig. S15 of the ESM). The presence of free Fe^{2+} may be taken as evidence for microbially-mediated pyrite oxidation (Hayakawa et al. 2013) and may serve as indirect evidence for chemolithotrophic and/or mixotrophic denitrification. Although the pyrite-bearing carbonate formations provide plenty of these niches in the rock matrix, turnover rates are likely to be very slow, since substrate diffusion is limited and thus the accessibility to microorganisms in the micritic limestones is also limited.

Conclusions

A strong spatial NO$_3^-$ variability in the groundwater of a fractured and karstified aquifer was observed. These variations can most likely be attributed to (1) local variances in agricultural practices within the capture zones of the

investigated groundwater monitoring wells, (2) a variable proportion of (often insufficiently known) karstic entryways below arable land and forests, and (3) fractional NO_3^- loss by denitrification in niches of the aquifer with near anoxic conditions within the otherwise oxygen-rich karstic formations of the recharge area. The multi-species (NO_3^-, NO_2^-) isotope approach allowed to better constrain the N turnover processes which potentially occur during transient storage of water and solutes in the temporarily saturated network of the epikarst or the fissure network of the phreatic zone. Karstic springs, as natural outlets of the entire conduit and fracture network of at least parts of the aquifer, are known to provide integrated information on water and solute inputs and transport along different flow paths. The information gained by the additional investigation of several monitoring wells in the recharge area turned out to be an important contribution for the development of the presented conceptual model on NO_3^- transport and turnover. This was due to the observed spatially varying chemical and hydraulic responses reflecting the connection of the monitoring wells to different parts of the fracture and fissure network which might favour transitory anoxic or suboxic conditions. Hence, the findings here suggest that future studies might need to consider possible impacts of near anoxic niches in the oxygen-rich karst recharge areas and to include not only karstic springs but also local groundwater observation points to better understand N transport and turnover dynamics within the karst groundwater systems.

References

Asante J, Dotson S, Hart E, Kreamer DK (2018) Water circulation in karst systems: comparing physicochemical and environmental isotopic data interpretation. Environ Earth Sci 77:421. https://doi.org/10.1007/s12665-018-7596-y

Ascott MJ, Gooddy DC, Wang L, Stuart ME, Lewis MA, Ward RS, Binley AM (2017) Global patterns of nitrate storage in the vadose zone. Nat Commun 8:1416. https://doi.org/10.1038/s41467-017-01321-w

Bakalowicz M (2005) Karst groundwater: a challenge for new resources. Hydrogeol J 13:148–160. https://doi.org/10.1007/s10040-004-0402-9

Benk SA, Yan L, Lehmann R, Roth V-N, Schwab VF, Totsche KU, Küsel K, Gleixner G (2019) Fueling diversity in the subsurface: composition and age of dissolved organic matter in the critical zone. Front Earth Sci 7(296). https://doi.org/10.3389/feart.2019.00296

Birk S, Liedl R, Sauter M (2004) Identification of localised recharge and conduit flow by combined analysis of hydraulic and physicochemical spring responses (Urenbrunnen, SW-Germany). J Hydrol 286:179–193. https://doi.org/10.1016/j.jhydrol.2003.09.007

Blanchette D, Lefebvre R, Nastev M, Cloutier V (2010) Groundwater quality, geochemical processes and groundwater evolution in the Chateauguay River watershed, Quebec, Canada. Can Water Resour J 35:503–526. https://doi.org/10.4296/cwrj3504503

Böhlke JK (2002) Groundwater recharge and agricultural contamination. Hydrogeol J 10:153–179. https://doi.org/10.1007/s10040-001-0183-3

Bourbonnais A, Altabet MA, Charoenpong CN, Larkum J, Hu H, Bange HW, Stramma L (2015) N-loss isotope effects in the Peru oxygen minimum zone studied using a mesoscale eddy as a natural tracer experiment. Glob Biogeochem Cycles 29:793–811. https://doi.org/10.1002/2014GB005001

Boy-Roura M, Menció A, Mas-Pla J (2013) Temporal analysis of spring water data to assess nitrate inputs to groundwater in an agricultural area (Osona, NE Spain). Sci Total Environ 452–453:433–445. https://doi.org/10.1016/j.scitotenv.2013.02.065

Brahana J, Tiong T, Mohammed A-Q, John M, Ralph D, Jozef L, Jonathan K, Eva S, Margaret D-S, Indrajeet C, Phillip H, Gregory T (2005) Quantification of hydrologic budget parameters for the vadose zone and epikarst in mantled karst. https://pubs.usgs.gov/sir/2005/5160/PDF/sir2005-5160part4.pdf. Accessed December 2020

Brandes JA, Devol AH (1997) Isotopic fractionation of oxygen and nitrogen in coastal marine sediments. Geochim Cosmochim Acta 61:1793–1801. https://doi.org/10.1016/S0016-7037(97)00041-0

Casciotti KL (2009) Inverse kinetic isotope fractionation during bacterial nitrite oxidation. Geochim Cosmochim Acta 73:2061–2076. https://doi.org/10.1016/j.gca.2008.12.022

Casciotti KL, McIlvin MR (2007) Isotopic analyses of nitrate and nitrite from reference mixtures and application to eastern tropical North Pacific waters. Mar Chem 107:184–201. https://doi.org/10.1016/j.marchem.2007.06.021

Codispoti LA, Brandes JA, Christensen JP, Devol AH, Naqvi SWA, Paerl HW, Yoshinari T (2001) The oceanic fixed nitrogen and nitrous oxide budgets: moving targets as we enter the Anthropocene? Sci Mar 65:85–105. https://doi.org/10.3989/scimar.2001.65s285

Cojean ANY, Jakob Z, Alan G, Claudia F, Fabio L, Lehmann Moritz F (2019) Direct O2 control on the partitioning between denitrification and dissimilatory nitrate reduction to ammonium in lake sediments. Biogeosciences 16:4705–4718. https://doi.org/10.5194/bg-16-4705-2019

Coplen TB, Bohke JK, Casciotti KL (2004) Using dual-bacterial denitrification to improve delta N-15 determinations of nitrates containing

mass-independent 17O. Rapid Commun Mass Spectrom 18:245–250. https://doi.org/10.1002/rcm.1318

D'Affonseca FM, Michael F, Cirpka Olaf A (2020) Combining implicit geological modeling, field surveys, and hydrogeological modeling to describe groundwater flow in a karst aquifer. Hydrogeol J 28:2779–2802

Dalsgaard T, Stewart FJ, Bo T, Loreto DB, Peter RN, Osvaldo U, Canfield DE, Delong EF (2014) Oxygen at nanomolar levels reversibly suppresses process rates and gene expression in anammox and denitrification in the oxygen minimum zone off northern Chile. MBio 5:e01966. https://doi.org/10.1128/mBio.01966-14

ECETOC (1988) Nitrate and drinking water. Eur Chem Ind Ecol Toxicol Centre. Brussels, Belgium

Einsiedl F (2005) Flow system dynamics and water storage of a fissured-porous karst aquifer characterized by artificial and environmental tracers. J Hydrol 312:312–321. https://doi.org/10.1016/j.jhydrol.2005.03.031

Einsiedl F, Mayer B (2005) Sources and processes affecting sulfate in a karstic groundwater system of the Franconian Alb, southern Germany. Environ Sci Technol 39:7118–7125. https://doi.org/10.1021/es050426j

Einsiedl F, Mayer B (2006) Hydrodynamic and microbial processes controlling nitrate in a fissured-porous karst aquifer of the Franconian Alb, southern Germany. 40:6697–6702. https://doi.org/10.1021/ES061129X

Einsiedl F, Maloszewski P, Stichler W (2005) Estimation of denitrification potential in a karst aquifer using the 15N and 18O isotopes of NO3⁻. Biogeochemistry 72:67–86. https://doi.org/10.1007/s10533-004-0375-8

Farnleitner AH, Wilhartitz I, Ryzinska G, Kirschner AKT, Stadler H, Burtscher MM, Hornek R, Szewzyk U, Herndl G, Mach RL (2005) Bacterial dynamics in spring water of alpine karst aquifers indicates the presence of stable autochthonous microbial endokarst communities. Environ Microbiol 7:1248–1259. https://doi.org/10.1111/j.1462-2920.2005.00810.x

Fidelibus MD, Balacco G, Gioia A, Iacobellis V, Spilotro G (2017) Mass transport triggered by heavy rainfall: the role of endorheic basins and epikarst in a regional karst aquifer. Hydrol Process 31:394–408. https://doi.org/10.1002/hyp.11037

Ford D, Williams PW (2007) Karst hydrogeology and geomorphology, 1st edn. Wiley, West Sussex, England

Goldscheider N (2005) Karst groundwater vulnerability mapping: application of a new method in the Swabian Alb, Germany. Hydrogeol J 13:555–564. https://doi.org/10.1007/s10040-003-0291-3

Granger J, Sigman DM (2009) Removal of nitrite with sulfamic acid for nitrate N and O isotope analysis with the denitrifier method. Rapid Commun Mass Spectrom 23:3753–3762. https://doi.org/10.1002/rcm.4307

Granger J, Wankel SD (2016) Isotopic overprinting of nitrification on denitrification as a ubiquitous and unifying feature of environmental nitrogen cycling. Proc Natl Acad Sci USA 113:E6391–E6400. https://doi.org/10.1073/pnas.1601383113

Granger J, Sigman DM, Prokopenko MG, Lehmann MF, Tortell PD (2006) A method for nitrite removal in nitrate N and O isotope analyses. Limnol Oceanogr 4:205–212. https://doi.org/10.4319/lom.2006.4.205

Granger J, Sigman DM, Lehmann MF, Tortell PD (2008) Nitrogen and oxygen isotope fractionation during dissimilatory nitrate reduction by denitrifying bacteria. Limnol Oceanogr 53:2533–2545. https://doi.org/10.4319/lo.2008.53.6.2533

Grathwohl P, Rügner H., Wöhling T., Osenbrück K., Schwientek M., Gayler S., Wollschläger U., Selle B., Pause M., Delfs JO, Grzeschik M, Weller U, Ivanov M, Cirpka OA, Maier U, Kuch B, Nowak W, Wulfmeyer V, Warrach-Sagi K, Streck T, Attinger S, Bilke L, Dietrich P, Fleckenstein JH, Kalbacher T, Kolditz O, Rink K, Samaniego L, Vogel HJ, Werban U, Teutsch G (2013) Catchments as reactors: a comprehensive approach for water fluxes and solute turnover. Environ Earth Sci 69:317–333. https://doi.org/10.1007/s12665-013-2281-7

Grimmeisen F, Lehmann MF, Liesch T, Goeppert N, Klinger J, Zopfi J, Goldscheider N (2017) Isotopic constraints on water source mixing, network leakage and contamination in an urban groundwater system. Sci Total Environ 583:202–213. https://doi.org/10.1016/j.scitotenv.2017.01.054

Gurdak JJ, Qi SL (2012) Vulnerability of recently recharged groundwater in principle aquifers of the United States to nitrate contamination. Environ Sci Technol 46:6004–6012. https://doi.org/10.1021/es300688b

Haber N, Hintemann T (2019) Agrarmeteorologie Baden-Württemberg [Agricultural meteorology Baden-Württemberg]. Landwirtsch. Technol. Augustenb. https://www.wetter-bw.de/Internet/AM/inetcntrBW.nsf/cuhome.xsp?imp=1YD95NVAG0&p1=KYIYU6XC4Y&p3=W3E8DV685Z&src=DXA7X04V99&p4=EZ5D5ZTI3K. Accessed 6 December 2020

Harbaugh AW (2005) MODFLOW-2005, the U.S. Geological Survey modular ground-water model: the ground-water flow process. US Geological Survey Techniques and Methods 6-A16, variously p

Harreß HM (1973) Hydrogeologische Untersuchungen im Oberen Gäu. Eberhard-Karls University Tübingen, Germany

Hartmann A, Goldscheider N, Wagener T, Lange J, Weiler M (2014) Karst water resources in a changing world: review of hydrological modeling approaches. Rev Geophys 52:218–242. https://doi.org/10.1002/2013RG000443

Hayakawa A, Hatakeyama M, Asano R, Ishikawa Y, Hidaka S (2013) Nitrate reduction coupled with pyrite oxidation in the surface sediments of a sulfide-rich ecosystem. J Geophys Res Biogeosci 118:639–649. https://doi.org/10.1002/jgrg.20060

Heberer T (2002) Occurrence, fate, and removal of pharmaceutical residues in the aquatic environment: a review of recent research data. Toxicol Lett 131:5–17. https://doi.org/10.1016/S0378-4274(02)00041-3

Heffernan JB, Albertin AR, Fork ML, Katz BG, Cohen MJ (2012) Denitrification and inference of nitrogen sources in the karstic Floridan aquifer. Biogeosciences 9:1671–1690. https://doi.org/10.5194/bg-9-1671-2012

Henson WR, Huang L, Graham WD, Ogram A (2017) Nitrate reduction mechanisms and rates in an unconfined eogenetic karst aquifer in two sites with different redox potential. J Geophys Res Biogeosci 122:1062–1077. https://doi.org/10.1002/2016JG003463

Herrmann M, Opitz S, Harzer R, Totsche KU, Küsel K (2017) Attached and suspended denitrifier communities in pristine limestone aquifers harbor high fractions of potential autotrophs oxidizing reduced iron and sulfur compounds. Microb Ecol 74:264–277. https://doi.org/10.1007/s00248-017-0950-x

Huebsch M, Fenton O, Horan B, Hennessy D, Richards KG, Jordan P, Goldscheider N, Butscher C, Blum P (2014) Mobilisation or dilution? Nitrate response of karst springs to high rainfall events. Hydrol Earth Syst Sci 18:4423–4435. https://doi.org/10.5194/hess-18-4423-2014

Husic A, Fox J, Adams E, Ford W, Agouridis C, Currens J, Backus J (2019) Nitrate pathways, processes, and timing in an agricultural karst system: development and application of a numerical model. Water Resour Res 55:2079–2103. https://doi.org/10.1029/2018WR023703

Husic A, Fox J, Adams E, Pollock E, Ford W, Agouridis C, Backus J (2020) Quantification of nitrate fate in a karst conduit using stable isotopes and numerical modeling. Water Res 170:115348. https://doi.org/10.1016/J.WATRES.2019.115348

Jones WK (2003) Physical structure of the epikarst. In: Jones WK, Culver DC, Herman JS (eds) Epikarst. Proceedings of the Symposium Held October 1 through 4, vol 2003. Karst Waters Institute, Shepherdstown, West Virginia, 160 pp

Jones AL, Smart PL (2005) Spatial and temporal changes in the structure of groundwater nitrate concentration time series (1935–1999) as demonstrated by autoregressive modelling. J Hydrol 310:201–215. https://doi.org/10.1016/j.jhydrol.2005.01.002

Katz BG (2012) Nitrate contamination in karst groundwater. In: White WB, Culver DC, Pipan T (eds) Encyclopedia of caves, 3rd edn. Academic, London, pp 756–760

Katz BG, Chelette AR, Pratt TR (2004) Use of chemical and isotopic tracers to assess nitrate contamination and ground-water age, Woodville karst plain, USA. J Hydrol 289:36–61. https://doi.org/10.1016/J.JHYDROL.2003.11.001

Kaufmann G, Gabrovšek F, Romanov D (2014) Deep conduit flow in karst aquifers revisited. Water Resour Res 50:4821–4836. https://doi.org/10.1002/2014WR015314

Kendall C, Aravena R (2000) Nitrate isotopes in groundwater systems. Springer US, Boston, MA, pp 261–297

Kendall C, Doctor DH (2005) Stable isotope applications in hydrologic studies. In: Drever JI (ed) Surface and ground water, weathering, and soils, 2nd edn. Elsevier, Amsterdam, pp 319–346

Kendall C, Elliott EM, Wankel SD (2007) Tracing anthropogenic inputs of nitrogen. In: Michener R, Lajtha K (eds) Stable isotopes in ecology and environmental science, 2nd edn. Blackwell, Oxford, UK, pp 376–428

Klueglein N, Kappler A (2013) Abiotic oxidation of Fe(II) by reactive nitrogen species in cultures of the nitrate-reducing Fe(II) oxidizer Acidovorax sp BoFeN1: questioning the existence of enzymatic Fe(II) oxidation. Geobiology 11:180–190. https://doi.org/10.1111/gbi.12040

Knowles R (1982) Denitrification. Microbiol Rev 46:43–70

Kuniansky EL, Spangler LE (2014) U.S. Geological Survey karst interest group proceedings. Carlsbad, NM

Kuypers MMM, Marchant HK, Kartal B (2018) The microbial nitrogen-cycling network. Nat Rev Microbiol 16:263–276. https://doi.org/10.1038/nrmicro.2018.9

Lakey B, Krothe NC (1996) Stable isotopic variation of storm discharge from a perennial karst spring, Indiana. Water Resour Res 32:721–731. https://doi.org/10.1029/95WR01951

Lehmann MF, Sigman DM, Berelson WM (2004) Coupling the $^{15}N/^{14}N$ and $^{18}O/^{16}O$ of nitrate as a constraint on benthic nitrogen cycling. Mar Chem 88:1–20. https://doi.org/10.1016/j.marchem.2004.02.001

Lian B, Yuan DX, Liu ZH (2011) Effect of microbes on karstification in karst ecosystems. Chin Sci Bull 56:3743–3747. https://doi.org/10.1007/s11434-011-4648-z

Liu Y, Zarfl CZ, Basu N, Schwientek M, Cirpka OA (2018) Contributions of catchment and in-stream processes to suspended sediment transport in a dominantly groundwater-fed catchment. Hydrol Earth Syst Sci Discuss. https://doi.org/10.5194/hess-2018-42

LUBW (2016) Sickerwasser- und Grundwasserneubildungraten im Untersuchungsgebiet [Infiltration and recharge rates within the area of interest]. Landesanstalt für Umwelt, Messungen und Naturschutz Baden-Württemberg, Karlsruhe, Germany

LUBW Landesanstalt für Umwelt (2017) Daten- und Kartendienst der LUBW. In: FFH-Mähwiesen. Landesanstalt für Umwelt, Messungen und Naturschutz Baden-Württemberg, Karlsruhe, Germany. https://udo.lubw.baden-wuerttemberg.de/public/. Accessed 6 December 2020

Matiatos I (2016) Nitrate source identification in groundwater of multiple land-use areas by combining isotopes and multivariate statistical analysis: a case study of Asopos basin (Central Greece). Sci Total Environ 541:802–814. https://doi.org/10.1016/j.scitotenv.2015.09.134

McIlvin MR, Altabet MA (2005) Chemical conversion of nitrate and nitrite to nitrous oxide for nitrogen and oxygen isotopic analysis in freshwater and seawater. Anal Chem 77:5589–5595. https://doi.org/10.1021/ac050528s

McIlvin MR, Casciotti KL (2010) Fully automated system for stable isotopic analyses of dissolved nitrous oxide at natural abundance levels. Limnol Oceanogr Methods 8:54–66. https://doi.org/10.4319/lom.2010.8.54

Medici G, West LJ, Banwart SA (2019) Groundwater flow velocities in a fractured carbonate aquifer-type: implications for contaminant transport. J Contam Hydrol 222:1–16. https://doi.org/10.1016/j.jconhyd.2019.02.001

Munch JC, Velthof GL (2007) Denitrification and agriculture. In: Biology of the nitrogen cycle. Elsevier, Amsterdam, pp 331–341

Musgrove M, Opsahl SP, Mahler BJ, Herrington C, Sample TL, Banta JR (2016) Source, variability, and transformation of nitrate in a regional karst aquifer: Edwards aquifer, central Texas. Sci Total Environ 568:457–469. https://doi.org/10.1016/j.scitotenv.2016.05.201

Nikolenko O, Jurado A, Borges AV, Knöller K, Brouy re S (2018) Isotopic composition of nitrogen species in groundwater under agricultural areas: a review. Sci Total Environ 621:1415–1432. https://doi.org/10.1016/j.scitotenv.2017.10.086

Niswonger RG, Panday S, Ibaraki M (2011) MODFLOW-NWT, A Newton formulation for MODFLOW-2005: U.S. Geological Survey Techniques and Methods 6-A37, 44 pp

Nolan BT, Stoner JD (2000) Nutrients in groundwaters of the conterminous United States, 1992–1995. Environ Sci Technol 34:1156–1165. https://doi.org/10.1021/es9907663

Page RM, Besmer MD, Epting J, Sigrist JA, Hammes F, Huggenberger P (2017) Online analysis: deeper insights into water quality dynamics in spring water. Sci Total Environ 599–600:227–236. https://doi.org/10.1016/j.scitotenv.2017.04.204

Panno SV, Hackley KC, Hwang HH, Kelly WR (2001) Determination of the sources of nitrate contamination in karst springs using isotopic and chemical indicators. Chem Geol 179:113–128. https://doi.org/10.1016/S0009-2541(01)00318-7

Perrin J, Jeannin PY, Zwahlen F (2003) Implications of the spatial variability of infiltration-water chemistry for the investigation of a karst aquifer: a field study at Milandre test site, Swiss Jura. Hydrogeol J 11:673–686. https://doi.org/10.1007/s10040-003-0281-5

Pipan T, Culver DC (2007) Epikarst communities: biodiversity hotspots and potential water tracers. Environ Geol 53:265–269. https://doi.org/10.1007/s00254-007-0640-y

Pollock DW (1994), User's guide for MODPATH/MODPATH-PLOT, version 3: a particle tracking post-processing package for MODFLOW, the U.S. Geological Survey finite-difference groundwater flow model, U.S. Geol. Surv. Open File Rep., 94-464, 248 pp

Pronk M, Goldscheider N, Zopfi J (2006) Dynamics and interaction of organic carbon, turbidity and bacteria in a karst aquifer system. Hydrogeol J 14:473–484. https://doi.org/10.1007/s10040-005-0454-5

Ravbar N (2013) Variability of groundwater flow and transport processes in karst under different hydrologic conditions. Acta Carsolog 42:327–338. https://doi.org/10.3986/ac.v42i2.644

Ravbar N, Goldscheider N (2009) Comparative application of four methods of groundwater vulnerability mapping in a Slovene karst catchment. Hydrogeol J 17:725–733. https://doi.org/10.1007/s10040-008-0368-0

Ravbar N, Engelhardt I, Goldscheider N (2011) Anomalous behaviour of specific electrical conductivity at a karst spring induced by variable catchment boundaries: the case of the Podstenjšek Spring, Slovenia. Hydrol Process 25:2130–2140. https://doi.org/10.1002/hyp.7966

Roco CA, Bergaust LL, Shapleigh PJ, Yavitt BJ (2016) Reduction of nitrate to nitrite by microbes under oxic conditions. Soil Biol Biochem 100:1–8. https://doi.org/10.1016/j.soilbio.2016.05.008

Sauter M, Geyer T, Kovács A, Teutsch G (2006) Modellierung der Hydraulik von Karstgrundwasserleitern: eine Übersicht—Herrn Professor Gerhard Einsele zum 80 [Modeling the hydraulics of karst

aquifers: an overview—dedicated to Professor Gerhard Einsele on the occasion of his 80th birthday]. Geburtstag gewidmet. Grundwasser 11:143–156. https://doi.org/10.1007/s00767-006-0140-0

Sawicki CR, Scaringelli FP (1971) Colorimetric determination of nitrate after hydrazine reduction to nitrite. Microchem J 16:657–672. https://doi.org/10.1016/0026-265X(71)90059-2

Schreiber F, Wunderlin P, Udert KM, Wells GF (2012) Nitric oxide and nitrous oxide turnover in natural and engineered microbial communities: biological pathways, chemical reactions, and novel technologies. Front Microbiol 3:372. https://doi.org/10.3389/fmicb.2012.00372

Schwab VF, Nowak ME, Elder CD, Trumbore SE, Xu X, Gleixner G, Lehmann R, Pohnert G, Muhr J, Küsel K, Totsche KU (2019) 14C-free carbon is a major contributor to cellular biomass in geochemically distinct groundwater of shallow sedimentary bedrock aquifers. Water Resour Res 55:2104–2121. https://doi.org/10.1029/2017WR022067

Schwarz MT, Oelmann Y, Wilcke W (2011) Stable N isotope composition of nitrate reflects N transformations during the passage of water through a montane rain forest in Ecuador. Biogeochemistry 102:195–208. https://doi.org/10.1007/s10533-010-9434-5

Simon KS, Benfield EF (2002) Ammonium retention and whole-stream metabolism in cave streams. Hydrobiologia 482:31–39. https://doi.org/10.1023/A:1021257822591

Smith LR, Böhlke JK, Garabedian SP, Revesz KM, Yoshinari T (2004) Assessing denitrification in groundwater using natural gradient tracer tests with 15N: in situ measurement of a sequential multistep reaction. Water Resour Res 40. https://doi.org/10.1029/2003WR002919

Stookey LL (1970) Ferrozine: a new spectrophotometric reagent for iron. Anal Chem 42:779–781. https://doi.org/10.1021/ac60289a016

Takaya N, Catalan-Sakairi MAB, Sakaguchi Y, Kato I, Zhou Z, Shoun H (2003) Aerobic denitrifying bacteria that produce low levels of nitrous oxide. Appl Environ Microbiol 69:3152–3157. https://doi.org/10.1128/AEM.69.6.3152-3157.2003

Ufrecht W, Hölzl S (2006) Salinare Mineral- und Thermalwässer im Oberen Muschelkalk (Trias) im Großraum Stuttgart: Rückschlüsse auf Herkunft und Entstehung mit Hilfe der 87Sr/86Sr-Strontium-Isotopie [Saline mineral and thermal waters in the Upper Muschelkalk (Triassic) in the greater Stuttgart area: conclusions on origin and formation with the help of the 87Sr / 86Sr strontium isotopy]. Zeitschr Dtsch Gesellsch Geowissenschaften 157:299–315. https://doi.org/10.1127/1860-1804/2006/0157-0299

Villinger E (1982) Hydrogeologische Aspekte zur geothermischen Anomalie im Gebiet Urach-Boll am Nordrand der Schwäbischen Alb (SW-Deutschland). In: Grundwasserbilanzen im Karstaquifer des Oberen Muschelkalks im Oberen Gäu (Baden-Württemberg) [Hydrogeological aspects of the geothermal anomaly in the Urach-Boll area on the northern edge of the SchwäbischeAlb (SW Germany). In: Groundwater balances in the karst aquifer of the Upper Muschelkalk in the Upper Gäu (Baden-Württemberg)]. Geol Jahrbücher Reihe C 32:43–61

Vystavna Y, Diadin D, Yakovlev V, Hejzlar J, Vadillo I, Huneau F, Lehmann MF (2017) Nitrate contamination in a shallow urban aquifer in East Ukraine: evidence from hydrochemical, stable isotopes of nitrate and land use analysis. Environ Earth Sci 76:463. https://doi.org/10.1007/s12665-017-6796-1

Wakida FT, Lerner DN (2005) Non-agricultural sources of groundwater nitrate: a review and case study. Water Res 39:3–16. https://doi.org/10.1016/j.watres.2004.07.026

Warren JK (2016) Salt dissolution and pointers to vanished evaporites: karst, breccia, nodules and cement. In: Evaporites. Springer, Cham, Switzerland, pp 613–761

Wegner C-EE, Gaspar M, Geesink P, Herrmann M, Marz M, Küsel K (2018) Biogeochemical regimes in shallow aquifers reflect the metabolic coupling of the elements nitrogen, sulfur, and carbon. Appl Environ Microbiol 85:e02346–e02318. https://doi.org/10.1128/AEM.02346-18

Wells NS, Hakoun V, Brouyère S, Knöller K (2016) Multi-species measurements of nitrogen isotopic composition reveal the spatial constraints and biological drivers of ammonium attenuation across a highly contaminated groundwater system. Water Res 98:363–375. https://doi.org/10.1016/j.watres.2016.04.025

Whelehan M, von Stockar U, Marison IW (2010) Removal of pharmaceuticals from water: using liquid-core microcapsules as a novel approach. Water Res 44:2314–2324. https://doi.org/10.1016/j.watres.2009.12.036

Williams PW (1983) The role of the subcutaneous zone in karst hydrology. J Hydrol 61:45–67. https://doi.org/10.1016/0022-1694(83)90234-2

Yue FJ, Li SL, Liu CQ, Zhao ZQ, Ding H (2017) Tracing nitrate sources with dual isotopes and long-term monitoring of nitrogen species in the Yellow River, China. Sci Rep 7:8537. https://doi.org/10.1038/s41598-017-08756-7

Zhou S, Zhang Y, Huang T, Liu Y, Fang K, Zhang C (2019) Microbial aerobic denitrification dominates nitrogen losses from reservoir ecosystem in the spring of Zhoucun reservoir. Sci Total Environ 651:998–1010. https://doi.org/10.1016/j.scitotenv.2018.09.160

Zhu X, Burger M, Doane TA, Horwath WR (2013) Ammonia oxidation pathways and nitrifier denitrification are significant sources of N_2O and NO under low oxygen availability. Proc Natl Acad Sci USA 110:6328–6333. https://doi.org/10.1073/pnas.1219993110

Publisher's note Springer Nature remains neutral with regard to jurisdictional claims in published maps and institutional affiliations.